Environmental Science Processes & Impacts

PAPER

View Article Online
View Journal | View Issue

Cite this: *Environ. Sci.: Processes Impacts*, 2018, **20**, 1593

Understanding interactions of organic nitrates with the surface and bulk of organic films: implications for particle growth in the atmosphere†

A. C. Vander Wall, [a] P. S. J. Lakey, [a] E. Rossich Molina,[c] V. Perraud, [a] L. M. Wingen, [a] J. Xu, [a] D. Soulsby, [b] R. B. Gerber, *[ac] M. Shiraiwa *[a] and B. J. Finlayson-Pitts *[a]

Understanding impacts of secondary organic aerosol (SOA) in air requires a molecular-level understanding of particle growth *via* interactions between gases and particle surfaces. The interactions of three gaseous organic nitrates with selected organic substrates were measured at 296 K using attenuated total reflection Fourier transform infrared spectroscopy. The organic substrates included a long chain alkane (triacontane, TC), a keto-acid (pinonic acid, PA), an amorphous ester oligomer (poly(ethylene adipate) di-hydroxy terminated, PEA), and laboratory-generated SOA from α-pinene ozonolysis. There was no uptake of the organic nitrates on the non-polar TC substrate, but significant uptake occurred on PEA, PA, and α-pinene SOA. Net uptake coefficients (γ) at the shortest reaction times accessible in these experiments ranged from 3×10^{-4} to 9×10^{-6} and partition coefficients (K) from 1×10^{7} to 9×10^{4}. Trends in γ did not quantitatively follow trends in K, suggesting that the intermolecular forces involved in gas–surface interactions are not the same as those in the bulk, which is supported by theoretical calculations. Kinetic modeling showed that nitrates diffused throughout the organic films over several minutes, and that the bulk diffusion coefficients evolved as uptake/desorption occurred. A plasticizing effect occurred upon incorporation of the organic nitrates, whereas desorption caused decreases in diffusion coefficients in the upper layers, suggesting a crusting effect. Accurate predictions of particle growth in the atmosphere will require knowledge of uptake coefficients, which are likely to be several orders of magnitude less than one, and of the intermolecular interactions of gases with particle surfaces as well as with the particle bulk.

Received 2nd August 2018
Accepted 17th October 2018

DOI: 10.1039/c8em00348c

rsc.li/espi

Environmental significance

The size and composition of atmospheric particles affects their light-scattering properties and ability to act as cloud condensation nuclei, which in turn affects Earth's radiative balance. Understanding how gases are taken up into particles to grow them to larger sizes is essential for accurately predicting their effects. This study shows that net uptake coefficients for unreactive gases such as organic nitrates into model organic substrates can be several orders of magnitude less than unity. Despite these small uptake coefficients, significant partitioning into organic semi-solids can occur, but trends in uptake do not necessarily follow those for partitioning. A comprehensive understanding of the interactions of gases with the surface compared to the bulk will help advance the current understanding of gas–particle interactions.

Introduction

Atmospheric aerosol particles are known to negatively impact air quality[1–4] and human health,[5–14] as well as to affect climate.[1,2,5,15] Organic aerosols are major contributors, including both primary emissions as well as secondary organic aerosol (SOA) particles formed in the oxidation of volatile organic compounds (VOC). Particles with sufficient size (~100 nm) scatter light significantly and act as cloud condensation nuclei, and their diameters strongly affect lung deposition.[16] However, mechanisms of nucleation and growth of organic particles to this size are not yet understood well.[17–26]

Particle growth has often been assumed to be governed by equilibrium partitioning between the gas and particle phases.[17,19,27–30] However, recent studies indicate that under some conditions, SOA particles may be of relatively high viscosity and hence subject to diffusion limitations and long equilibration

[a]Department of Chemistry, University of California, Irvine, Irvine, CA 92697, USA. E-mail: bjfinlay@uci.edu; bgerber@uci.edu; m.shiraiwa@uci.edu; Fax: +1 949 824-2420; Tel: +1 949 824-7670

[b]Department of Chemistry, University of Redlands, 1200 East Colton Ave, Redlands, CA 92373, USA

[c]Institute of Chemistry, Fritz Haber Research Center, Hebrew University of Jerusalem, Jerusalem 91904, Israel

† Electronic supplementary information (ESI) available. See DOI: 10.1039/c8em00348c

timescales.[31–49] In this case, the mechanism may not be governed by quasi-equilibrium growth,[50] but rather by a kinetically-controlled, diffusion limited mechanism.[51–56] For example, Perraud *et al.*[39] showed that for particles formed by the oxidation of α-pinene by ozone and NO_3 radical, the nitrate concentration in the particles was not consistent with equilibrium partitioning between the gas and particle phases. Additionally, Zaveri *et al.*[57] showed that both the growth and evaporation kinetics of bimodal SOA particles were best reproduced by a semi-solid scenario. A recent study by Wang *et al.*[58] showed that the dynamics of SOA formation and growth should take into account a number of processes that occur simultaneously, rather than a quasi-equilibrium approach.

Slow diffusion throughout the particle due to a glassy or semi-solid phase state is believed to limit the rate of uptake of incoming gas phase into the underlying layers of the particle,[41] and it is also expected to change the evaporation kinetics of molecules back into the gas phase. For example, Vaden and co-workers[33] investigated the adsorption of insoluble hydrophobic compounds including pyrene and dioctylphthalate (DOP) onto dry SOA generated from the ozonolysis of α-pinene. Single particle measurements showed that these compounds coated the SOA particle surface, forming either a solid nodule and aspherical particles (pyrene) or layered particles (DOP). In both cases, the evaporation of underlying SOA was slowed down. Effects of viscosity and diffusion were also observed in a number of recent studies involving uptake onto organic aerosol and aerosol model systems or proxies using atmospherically relevant gases including organics such as levoglucosan ($C_6H_{10}O_5$)[59] and polycyclic aromatic hydrocarbons,[60–62] water (H_2O),[49,63–66] ozone (O_3),[41,67–70] hydroxyl radicals (OH),[70–72] nitrate radicals (NO_3),[73] hydroperoxyl radicals (HO_2),[74] ammonia (NH_3)[75–77] and amines.[78–81]

A number of approaches have been developed to parameterize both physical and chemical interactions of gases with atmospherically relevant particle systems.[41,68,82–85] The strength of the initial interaction of the gas with the surface must depend at a fundamental level on both the structures and functional groups of the gas and the surface, and such properties must ultimately provide the bedrock for model parameterizations. For example, to a first approximation, it is expected that a polar gas with hydrogen-bonding potential would be taken up on a polar surface with similar functional groups more readily than on a non-polar surface.

The interaction of a gas with a condensed phase where no reaction occurs involves a number of individual steps:[23,86] (1) diffusion of the gas to the surface; (2) adsorption at the surface; and (3) incorporation into the bulk *via* mass transport from the surface layer. The second step is often referred to as surface accommodation and the third as bulk accommodation. The efficiency of each step is generally expressed in terms of accommodation coefficients. The surface accommodation coefficient (α_s) is the number of molecules adsorbed to the surface for times longer than a single scattering event divided by the number of gas–surface collisions, while the bulk accommodation coefficient (α_b) is the ratio of the number of molecules taken up into the bulk to the number of gas–surface collisions. Experimentally, a net gas uptake coefficient (γ) is usually measured, where γ is the ratio of the total number of molecules removed from the gas phase (or the total number incorporated into the condensed phase) to the number of gas–surface collisions. This net uptake coefficient reflects a combination of all of the processes above, and in the case of reactive uptake, the chemistry as well.

In any event, there should be a range of uptake coefficients reflecting the gas–surface attractive forces. It should be noted

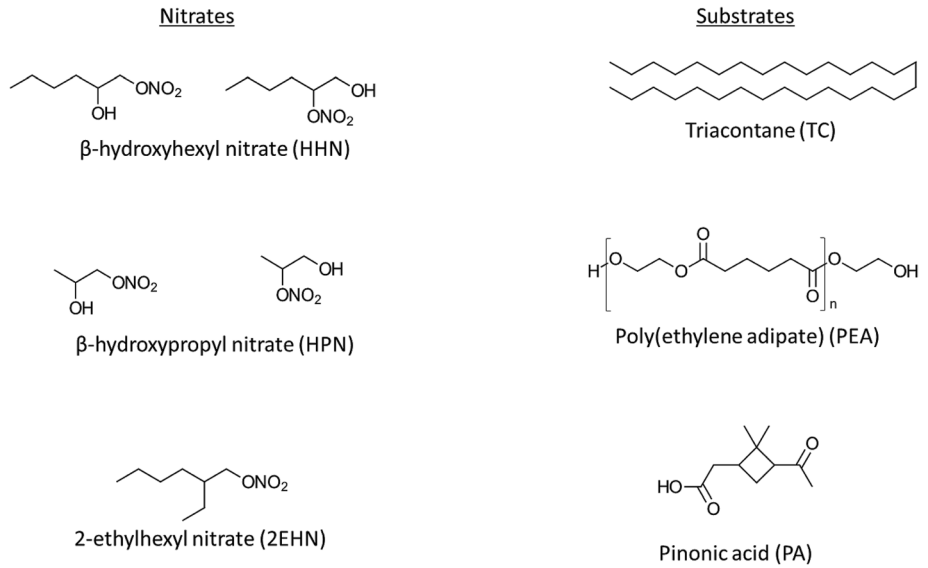

Fig. 1 Structures of the gas phase organic nitrates β-hydroxyhexyl nitrate (HHN), β-hydroxypropyl nitrate (HPN), and 2-ethylhexyl nitrate (2EHN), and the organic thin film substrates triacontane (TC), poly(ethylene adipate) (PEA), and pinonic acid (PA). SOA is not shown since it is a complex mixture.

that the intermolecular forces between an incoming gas and the surface of a particle may not be the same as those experienced by the gas when taken up into the bulk. A comprehensive parameterization involving detailed gas–surface intermolecular interactions remains challenging, in part due to the lack of available experimental data.

The goal of the present experiments was to probe the relationship between different gas–surface interactions and net uptake coefficients as well as the bulk solubilities of the gas. Organic nitrates are known to be formed by the OH radical oxidation of VOCs in the presence of NO_x and are also known to be important products in NO_3 radical oxidation reactions.[87–98] Alkyl and multifunctional organic nitrates, including hydroxynitrates, have also been measured in both ambient air and particles.[99–105] Three different organic nitrates with varying functionalities, structures, and vapor pressures, as well as various organic film substrates were studied. The nitrates, shown in Fig. 1, include two isomeric β-hydroxynitrate mixtures, β-hydroxypropyl nitrate (HPN) and β-hydroxyhexyl nitrate (HHN), and 2-ethylhexyl nitrate (2EHN, an alkyl nitrate). Organic nitrates are spectroscopically unique, exhibiting strong absorptions in the infrared region (specific $-ONO_2$ stretches are at 850 cm^{-1} for the N–O stretch, 1280 cm^{-1} for the symmetric NO_2 stretch, and 1630 cm^{-1} for the asymmetric NO_2 stretch).[90,106] This facilitated following uptake and desorption of the nitrates *in situ* and in real time using attenuated total reflection Fourier transform infrared spectroscopy (ATR-FTIR). The substrates (Fig. 1) include a non-polar long chain alkane (triacontane, TC), an amorphous ester oligomer (poly(ethylene adipate) di-hydroxy terminated, PEA), a keto-acid (pinonic acid, PA), and SOA from α-pinene ozonolysis. The alkane might be considered a model for primary organic aerosol,[107] while the keto-acid and ester are representative of functionalities found in SOA.[108–113] Both net initial uptake and partition coefficients were measured to provide insight into interactions of gases with surfaces compared to the bulk, and desorption was also captured to understand diffusivity back into the gas phase. Kinetic modeling and quantum chemical calculations were applied to provide additional molecular level insight into these interactions.

Experimental

Methods

Fig. 2 shows a schematic diagram of the ATR-FTIR cell. For each uptake experiment, a Ge crystal coated with the target substrate was placed in the cell (total volume ~ 2 cm^3) in the sampling compartment of an FTIR spectrometer (Nicolet 6700). The spectrum of each sample was acquired using 4 co-added scans with a resolution of 8 cm^{-1}, yielding a time resolution of 1 data point approximately every 3 seconds. The film alone was first exposed to 60 ± 5 cm^3 min^{-1} clean, dry air from a purge air generator (Parker-Balston, model 75-62) for 15–300 seconds to dry the film and to bring any spreading that might occur under a gas flow to a steady-state before the addition of the nitrate. The organic nitrate ($RONO_2$) was then introduced into the ATR cell by flowing clean, dry air at a flow rate of 60 ± 5 cm^3 min^{-1}

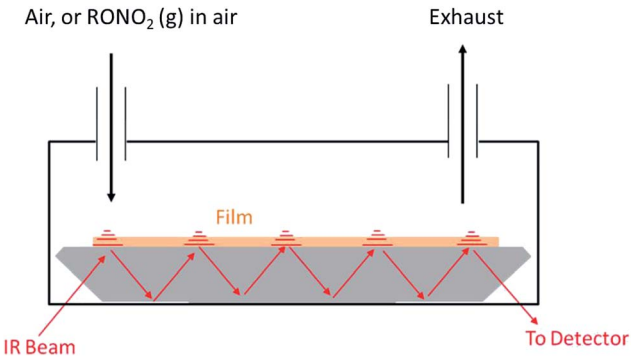

Fig. 2 Schematic of the ATR uptake apparatus.

over the pure liquid of each organic nitrate contained in a glass trap at room temperature. The gas-phase concentrations were assumed to be equivalent to the saturation vapor pressure of the organic nitrate. The trap was replenished daily with fresh organic nitrate (synthesized hydroxynitrates were stored in a freezer under N_2 (g)). In some cases, the organic nitrate signal in the IR decreased over the course of a day, indicating there may have been some decomposition in the trap. When decomposition was observed, only data from the first run of the day were used. Additional experiments where the time the film was exposed to the organic nitrate was doubled also showed stability of the organic nitrate signal, indicating decomposition was minimal over the length of the experiments.

The 2EHN was purchased and used as received. The HHN and HPN were synthesized by scaling up the method of Cavdar and Saracoglu.[114] In brief, epoxyhexane or epoxypropane were reacted with bismuth(III) nitrate·$5H_2O$ in a 1 : 2 mole ratio (typical amounts were on the order of 10^{-2} moles), in dichloromethane as the solvent. The reaction was carried out with constant stirring for 16–24 hours at room temperature under N_2 (g), after which the solvent was evaporated off *in vacuo* (Wheaton, SPIN-VAP). The liquid product was then purified using a silica gel column, with a solvent system of 2 : 1 ethyl acetate : hexanes, and again the solvent was removed using a roto-vap. As shown in the ESI,† the resulting liquid product was characterized using FTIR (Nicolet 6700, Fig. S1†), GC-MS (Agilent 7890a GC system with a 5975C MS detector, Fig. S2†), and ^1H NMR (Bruker DRX500, 500 MHz, in $CDCl_3$ with 0.05% tetramethylsilane, Fig. S3†), with final purities of ~87–90% for both HPN and HHN estimated from the NMR data. Impurities were identified as residual solvent and the corresponding di-alcohol by comparison to pure standards.

In addition, the purity of the gas-phase organic hydroxynitrates (HHN and HPN) from the headspace of the trap was examined by direct analysis in real-time mass spectrometry (DART-MS) using a triple quadrupole mass spectrometer (Waters, Xevo TQ-S) with a DART ionization source (Ion-Sense, DART SVP with Vapur® Interface). Since DART is an ambient ionization method, quantification is difficult but identification of the nitrates and some impurities using this method is reliable. Conditions used were the following: helium gas flow, 3.1 L min^{-1}; grid electrode voltage, 350 V; DART temperature,

25 °C. DART-MS measurements were performed at low temperature to minimize thermal decomposition of the organic nitrates.[115,116] All mass spectra were recorded in the positive ion mode for m/z ranging from 25 to 400 amu. The mass spectra for both HPN and HHN, as well as the mass spectra for the corresponding di-alcohols, are shown in Fig. S4.† The predominant peaks in the DART spectra are due to $[2M + H - NO_2]^+$ at m/z 197 and 281 for HPN and HHN, respectively. There was little to no evidence for the corresponding di-alcohol in the gas-phase above the liquid.

FTIR analysis

These organic nitrates were chosen because of their range of vapor pressures, different functional groups and spectral signatures in the IR. The characteristic peaks of the nitrate were monitored over time (1280 and 1630 cm^{-1}) along with the carbonyl peaks of the organic film (1700–1730 cm^{-1}) while the gas-phase nitrate flowed over the film. For TC, which has no carbonyl functional group, the C–H peak at 2915 cm^{-1} was followed. After the organic nitrate signal reached equilibrium, the flow was replaced with 60 ± 5 cm^3 min^{-1} clean, dry air to follow the desorption of the tracer as a function of time.

To quantify the amount of nitrate taken up into the film in units of molecules per cm^2, FTIR cross-sections for the organic nitrate tracers (1280 cm^{-1}) and the organic substrates (–C=O stretch at 1700–1730 cm^{-1}) were obtained using solution standards of known concentrations. Details on the cross-section calculations are found in the ESI,† and the cross sections for all compounds are listed in Table S1.† Pinonic acid gives a different signal in the solid phase (film) than in the liquid (see Fig. S5†), and details on this quantification are given in the ESI.†

To calculate the mole ratio of nitrate to carbonyl groups for each substrate, eqn (1) was used:

$$\frac{A_{nit}}{A_{C=O}} \times \frac{l_{C=O} \times \sigma_{C=O}}{l_{nit} \times \sigma_{nit}} = \frac{n_{nit}}{n_{C=O}} \quad (1)$$

In eqn (1), A_{nit} and $A_{C=O}$ are the IR absorbances for the organic nitrate and the carbonyl of the substrate, respectively, σ is the absorption cross-section (cm^2 mol^{-1}, base 10), and l is the pathlength (cm) probed in the film at the selected wavenumbers for the carbonyl and the organic nitrate. In eqn (1), n_{nit} and $n_{c=o}$ are the number of moles of nitrate and carbonyl, respectively. The pathlength determination for the ATR beam is described in the ESI, Section 2.† Substrate films were prepared to allow penetration of the IR beam throughout the entire film if evenly spread over the crystal, but due to inhomogeneity in the distribution of the films over the crystal surfaces (Fig. S6†), this may not be the case in some regions of the film.

For uptake coefficients, the amount of nitrate taken up was determined from the organic nitrate peak height using eqn (2),

$$\frac{A_{nit}}{\sigma_{nit}} \times N_A = \{-ONO_2\} \quad (2)$$

where A_{nit} is the absorbance of the organic nitrate, σ_{nit} is the cross section of the organic nitrate in cm^2 mol^{-1} (base 10), N_A is Avogadro's number, and $\{-ONO_2\}$ is the amount of nitrate in the film. Although $\{-ONO_2\}$ is expressed as the number of $-ONO_2$ per cm^2, it is the column integrated nitrate and includes both surface and bulk contributions. By plotting the concentration over time as the film is exposed to the organic nitrate and subsequently taking the initial slope of the initial data points (t < 20 s), the initial net uptake coefficient (γ) was quantified by eqn (3):

$$\gamma = \frac{R_0}{[gas] \times \sqrt{\frac{RT}{2\pi M}}} \quad (3)$$

where R_0 is defined as the initial rate of uptake. Lastly, partition coefficients K were calculated using eqn (4),

$$K = \frac{[-ONO_2]_{film}}{[-ONO_2]_{air}} \quad (4)$$

where $[-ONO_2]_{film}$ and $[-ONO_2]_{air}$ are the concentrations of organic nitrate in the film and in air, respectively, in units of moles per L. The concentration in air was estimated using the saturation vapor pressure. The concentration of nitrate in the film, $[-ONO_2]_{film}$, takes into account the swelling of the film (see below) on uptake of the organic nitrate, eqn 5:

$$\frac{\frac{A_{nit}}{l_{nit} \times \sigma_{nit}}}{\frac{A_{C=O}}{l_{C=O} \times \sigma_{C=O}} + \frac{A_{nit}}{l_{nit} \times \sigma_{nit}}} = \frac{n_{nit}}{n_{C=O} + n_{nit}} \quad (5)$$

The $n_{C=O}$ (moles of C=O) is converted into n_{Sub} (moles of substrate) using the number of carbonyl groups in each substrate molecule ($N_{C=O}/N_{Sub}$ = 2 for PA, 12 for PEA, and assuming 2 for SOA):[108,109]

$$n_{C=O} \times \frac{N_{Sub}}{N_{C=O}} = n_{Sub} \quad (6)$$

Moles of substrate and moles of nitrate are converted to volume (in units of L) using the molecular weight (M, assuming 200 g mol^{-1} for SOA),[108–110] and the densities in units of g L^{-1} (using 1.2 × 10^3 g L^{-1} for SOA):[117]

$$\frac{n_{nit}}{n_{Sub} \times \frac{M_{Sub}}{\rho_{Sub}} + n_{nit} \times \frac{M_{nit}}{\rho_{nit}}} = [-ONO_2]_{film} \quad (7)$$

Organic film preparation and secondary organic aerosol generation/impaction

Films were created by dissolving the pure solid in solvent (hexanes, dichloromethane, methanol, or acetonitrile) and spreading a known volume (5–20 μL) of the solution onto the exposed face of the ATR crystal. The solvent was removed using a flow of dry N_2 (g) until only the dry solid remained.

SOA from the ozonolysis of α-pinene was generated in a large volume, slow flow, stainless steel aerosol flow reactor described

in detail elsewhere[118] using initial concentrations of 250 ppb α-pinene and 250–350 ppb O_3. The details on α-pinene SOA generation are presented in the ESI† and an example of the size distribution of the particles generated in the flow reactor is shown in Fig. S7.† The polydisperse SOA particles formed in the flow reactor were collected onto a Ge ATR crystal using a custom-designed impactor with a 50% cut-off diameter of 240 nm.[38] The particles were sampled at a total flow of 30 L min^{-1} for 10–20 minutes at the end of the reactor corresponding to a reaction time of 31 minutes.

Theoretical calculations

Relevant physical properties of these organic nitrates (molecular weight, vapor pressure, and dipole moment) are given in Table 1. The dipole moment of each organic nitrate (including both OH-terminated and nitrate-terminated isomers for HHN and HPN) was calculated as described below. Their vapor pressures were estimated using two group contribution methods.[119–121] The vapor pressures for 2EHN and HPN are on the border between VOC and intermediate VOC (IVOC), while the lower vapor pressure of HHN classifies it as an IVOC.[122] Note that for HHN and HPN there are two isomers generated in the synthesis (hydroxy-terminated and nitrate-terminated). Because these have different vapor pressures, the average of the two isomers was used to calculate gas phase concentrations for the hydroxynitrates. While the predicted vapor pressures differ slightly between the two methods, these differences are relatively small and do not change the general trends in the reported results.

Geometry optimization, frequency calculations, and dipole moments for the organic nitrates were performed at the level of B3PW91 (ref. 123 and 124)/aug-cc-pVDZ.[125] To test the adequacy of the method for the dipole moments, isobutyl nitrate (IBN) was used as a test compound. The dipole moment of IBN obtained here (3.7243 D) is in excellent agreement with a previously reported value (3.6806 D at the level of B3PW91/6-31G(d)),[126] and the values for the studied organic nitrates also agree reasonably well with calculated dipole moments for other organic nitrate species.[127] All calculations were performed using the Q-CHEM 4.3 program package.[128]

The structures of the nitrate–PEA complexes were built using Packmol[129] software. These structures were optimized using Gaussian09 (D 0.1) software[130] and the geometries were confirmed as minima by the absence of imaginary frequencies. Counterpoise correction[131] was included to account for the Basis Set Superposition Error (BSSE) in binding energies nitrate–PEA calculations. Density functional theory with the hybrid functional B3LYP[132,133] using the 6-31+G(d) Pople basis set,[134] and with Grimme's D3 correction for dispersion[135] were employed for the energetics and structure calculations of the complex. This method has the capability to describe both the electrostatic interactions due to the partial charges on the atoms and the very significant dispersion interactions.

KM-GAP model

The uptake of organic nitrates into the three different substrates (PA, PEA, and SOA) was investigated using the kinetic multi-layer model of gas–particle interactions in aerosols and clouds (KM-GAP).[136] This model is based on fundamental physical processes and explicitly treats the adsorption and desorption of the organic nitrate to and from the surface of the substrate, partitioning of the adsorbed organic nitrate into the bulk of the substrate, and bulk diffusion of the substrate and nitrate. The bulk was treated with 100 layers which could each grow and shrink as molecules diffused in and out of them, consequently the total thickness of the bulk increased and decreased due to condensation and evaporation. The bulk diffusion coefficient of the nitrate ($D_{b,nit}$) and substrate ($D_{b,sub}$) were treated to be composition-dependent using Vignes-type equations[64,67] as described in the ESI, Section 4.† The partition coefficients from the experiments were used as fixed model inputs and the best fit film thicknesses were calculated from the model. The model-predicted thicknesses are constrained to a small range of values based on the experimental data provided. For PA and PEA, they are larger than those calculated assuming the substrate is distributed equally over the entire surface of the crystal. This is reasonable since the solutions of PA and PEA did not dry uniformly, with more material located in the center of the crystal (Fig. S6†). The model-predicted thickness for SOA is smaller than if spread equally. The impactor deposits SOA unevenly,[38] being weighted towards the center (Fig. S6†), and the amount deposited to give sufficient carbonyl signals was about an order of magnitude greater than for PEA and PA. The absolute number of nitrate molecules measured in the SOA may therefore have been underestimated, which would lead to an underestimate of the model-predicted film thickness. However, this does not change the conclusions.

Table 1 Molecular properties of the organic nitrates at 25 °C

Organic nitrates	MW (g mol^{-1})	ρ (g mL^{-1})	Vapor pressure using Moller[120,121] (Pa)	Vapor pressure[d] using SIMPOL.1 (ref. 119) (Pa)	Dipole moment (D)
HHN	163	1.1	0.35[a] 0.65[b] Average[c] = 0.50 ± 0.21	0.85	4.6220[a] 2.8393[b]
HPN	121	1.2	12[a] 35[b] Average[c] = 24 ± 16	16	4.6191[a] 4.7683[b]
2EHN	175	0.96	14	18	3.9216

[a] Hydroxy-terminated isomer. [b] Nitrate-terminated isomer. [c] Error bars are ±1σ. [d] SIMPOL.1 does not distinguish between isomers.

Reagents

Reagents and sources were as follows: dodecane (Sigma Aldrich, ≥99%), methanol (EMD Millipore, ≥99.9%), acetonitrile (EMD Millipore, ≥90%), epoxyhexane (Sigma-Aldrich, 97%), epoxypropane (Sigma-Aldrich, ≥99%), bismuth(III) nitrate·$5H_2O$ (Sigma-Aldrich, 98%), dichloromethane (EMD Millipore, ≥99.9%), chloroform-D (with 0.05% by volume tetramethylsilane, Cambridge Isotope Laboratories Inc., 99.8%), (+)-α-pinene (Sigma-Aldrich, ≥99%), hexanes (VWR Analytical, >98.5%), dichloromethane (Macron, ≥99.5%), ethyl acetate (EMD Chemical Inc., >99.5%), triacontane (Sigma-Aldrich, 98%), L-(+)-tartaric acid (Sigma-Aldrich, ≥99.5%), poly(ethylene adipate) di-hydroxy terminated (Sigma-Aldrich, average MW 1000), *cis*-pinonic acid (Sigma-Aldrich, 98%), 2-ethylhexyl nitrate (Sigma-Aldrich, 97%), valeric acid (Sigma-Aldrich, ≥99%), 2-nonanone (Sigma-Aldrich, ≥99%), propanediol (Sigma-Aldrich, ≥99.5%), hexanediol (Sigma-Aldrich, 98%), N_2 (Praxair, 99.999%), and O_2 (Praxair, 99.993%).

Results and discussion

ATR-FTIR spectra

Fig. 3a shows the ATR-FTIR spectra for the solid film substrates before exposure to the organic nitrates, and Fig. 3b shows typical spectra for each substrate after exposure to 5 ppm gaseous HHN. Similar spectra showing each substrate after exposure to 250 ppm HPN or 140 ppm 2EHN can be found in Fig. S8.† Note that the saturation vapor pressure of HHN is much lower than that of HPN or 2EHN, limiting the HHN concentration that can be generated in the gas phase. Despite the two orders of magnitude lower concentration, uptake of HHN is still clearly evident onto SOA, PA and PEA. As seen in Fig. 3 and S8,† there was no observed uptake onto TC, and uptake onto the Ge crystal itself was minimal for all three organic nitrates.

The lack of uptake of all the organic nitrates on TC is not surprising. With the absence of polar interactions or hydrogen-bonding between the gas and the hydrocarbon surface, the dispersion forces may simply be too weak to result in any significant uptake onto the TC (we use here the terminology of "van der Waals' interactions" for all weak non-covalent forces, including hydrogen-bonding, and use "dispersion interactions" specifically for forces due to induced dipoles).[137] In contrast, there was significant uptake observed for the organic nitrates onto PA, PEA and SOA.

Fig. 4 shows typical data for the time-dependent uptake of the three organic nitrates on SOA, PA and PEA respectively, calculated using eqn (2) above. The curves are best fits from the KM-GAP model,[136] discussed in detail below. In all cases, there is a rapid initial uptake which then rises to a plateau, at which point there is no further net uptake. The concentrations of the organic nitrates are significant, reaching as high as 3×10^{16} molecules per cm^2 for HHN on PA. The amount taken up is much larger than a monolayer ($\sim 10^{14}$ molecules per cm^2), which suggests either (a) that the organic nitrates adsorbed and created a film along the surface approximately 100 monolayers thick, or (b) that the organic nitrates are not simply adsorbed onto the surface but are penetrating and diffusing throughout the organic film. The former seems unlikely, and diffusion through the organic films is feasible given the timescales of the experiments and estimated thicknesses of the films. As discussed below, this is also supported by relatively slow desorption of the nitrates out of the film.

Net uptake coefficients

From the initial rapid uptake, a net uptake coefficient γ can be obtained. These are summarized in Table 2, and shown in Fig. 5. In the framework proposed by Pöschl, Rudich and Ammann[86] and Kolb *et al.*,[23] these would be equivalent to bulk accommodation coefficients (α_b) because the nitrate in the entire film is interrogated by IR. In the application of the

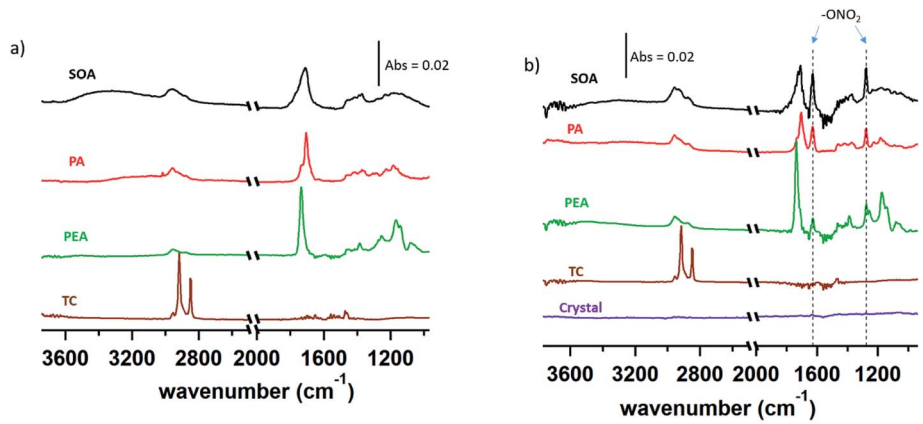

Fig. 3 ATR-FTIR spectra for (a) SOA, pinonic acid (PA), poly(ethylene) adipate (PEA), and triacontane (TC), and (b) after exposure to gaseous HHN (5 ppm) once equilibrium was reached (450–1050 seconds), as well as the spectra for exposure of the clean crystal to the organic nitrate. TC spectra were multiplied by a factor of 0.25, and PEA spectra by a factor of 0.5 to display them on the same scale as the other spectra. Dashed lines indicate the $-ONO_2$ signals characteristic of organic nitrates. The region between 2500–2000 cm^{-1} is not shown due to variations in the CO_2 (g) in the sampling compartment.

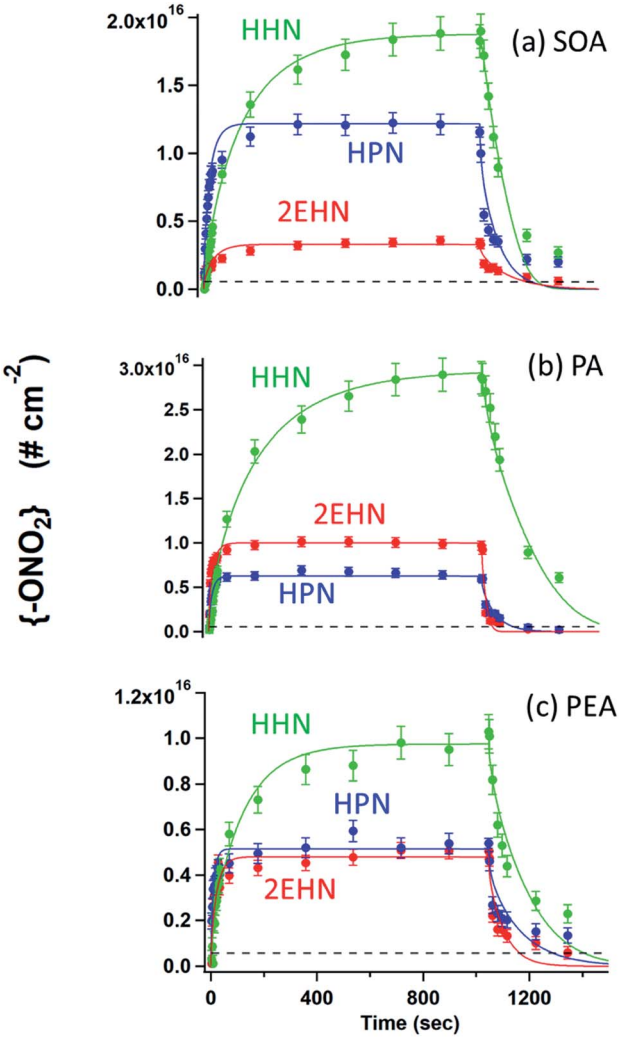

Fig. 4 Concentrations of organic nitrates {$-ONO_2$} from eqn (2) in number per cm^2 after exposure of (a) SOA, (b) PA and (c) PEA to gaseous HHN (5 ppm), HPN (250 ppm), and 2EHN (140 ppm). The dashed black line indicates the experimentally-determined limit of detection for the nitrates. Solid lines are best fits from the KM-GAP model. Error bars are $\pm 2\sigma$ on the experimental data points determined from the uncertainty in the measured absorption cross section of HHN, HPN and 2EHN.

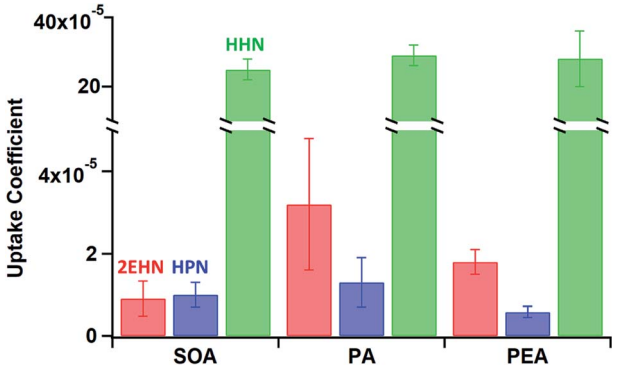

Fig. 5 Initial uptake coefficients for the organic nitrates into SOA, PA, and PEA. Error bars are $\pm 1\sigma$ from the average of multiple experiments for each nitrate.

KM-GAP model discussed below, the surface mass accommodation coefficients (α_s) were taken to be one, and diffusion of the gas to the surface is not limiting under our conditions.

The limited number of data points in this initial time frame gives rise to significant error bars, and may underestimate the rate of uptake as the films begin to take up the organic nitrate and some re-evaporation from the film occurs. As discussed earlier, the gas-phase organic nitrate concentrations may be overestimated and the substrate films may not be homogeneous in thickness, which would also result in underestimates of the uptake coefficients. However, this approach should provide reliable relative rates for the different organic nitrates and substrates, as well as order-of-magnitude absolute values that can be used to provide insight into molecular interactions between the gas and the surface films.

As seen in Fig. 5, HHN has by far the largest net uptake coefficient for all three substrates, with values over an order of magnitude higher than those of HPN and 2EHN. This is not surprising as HHN has the largest capacity for intermolecular interactions, possessing both the additional hydroxyl group for hydrogen bonding and the longer carbon backbone for dispersion interactions. In sharp contrast, uptake of HHN is minimal on TC as well as on the clean crystal (Fig. 3). Hence, hydrogen bonding and other van der Waals' forces with specific

Table 2 Average net uptake coefficients (γ) and partition coefficients (K)

Organic nitrates	Substrates	Average uptake coefficient[a] (γ)	Average partition coefficient[a] (K)
HHN	SOA	$(2.5 \pm 0.2) \times 10^{-4}$	$(1.5 \pm 0.2) \times 10^{7}$
	PA	$(2.9 \pm 0.3) \times 10^{-4}$	$(1.8 \pm 0.2) \times 10^{7}$
	PEA	$(2.8 \pm 0.8) \times 10^{-4}$	$(7.3 \pm 1.8) \times 10^{6}$
HPN	SOA	$(1.0 \pm 0.3) \times 10^{-5}$	$(3.4 \pm 1.2) \times 10^{5}$
	PA	$(1.3 \pm 0.6) \times 10^{-5}$	$(2.4 \pm 0.7) \times 10^{5}$
	PEA	$(5.8 \pm 1.3) \times 10^{-6}$	$(9.5 \pm 3.5) \times 10^{4}$
2EHN	SOA	$(9.0 \pm 4.3) \times 10^{-6}$	$(1.7 \pm 0.1) \times 10^{5}$
	PA	$(3.2 \pm 1.6) \times 10^{-5}$	$(3.3 \pm 1.1) \times 10^{5}$
	PEA	$(1.8 \pm 0.3) \times 10^{-5}$	$(1.1 \pm 0.1) \times 10^{5}$

[a] Error bars are statistical $\pm 1\sigma$ from the average of multiple experiments.

functional groups on the substrates must play a significant role to anchor the incoming gas phase molecule onto PA, PEA and SOA.

These measured uptake coefficients are orders of magnitude less than one. This is reasonable given the range of previously reported uptake coefficients for both reactive and non-reactive uptake. For an example of reactive uptake, Fairhurst *et al.*[78,79] reported that for the uptake of various amines and ammonia with a series of dicarboxylic acids, net reactive uptake coefficients ranged from 0.7 to less than 10^{-6}. Additionally, a previous study by Donaldson *et al.*[138] showed that the unreactive uptake of a range of organic vapours onto organic films of oleic acid or squalene ranged from $\sim 10^{-2}$ to less than 10^{-5}.

Calculations of the structures and binding energies for complexes of the nitrates with the substrates can lend insight into the forces that provide the initial anchor for the incoming nitrate. Binding energy calculations were carried out for complexes of one or two gas phase nitrate molecules (2EHN, HPN and HHN) with one PEA substrate subunit. While PEA has an average molecular weight of 1000 g mol^{-1} and thus contains 5–6 subunits, one PEA subunit was used to represent the substrate due to computational constraints.

Fig. 6 shows the optimized structures for one nitrate molecule interacting with one PEA subunit for all the organic nitrates. The binding energies are summarized in Table S3.† As seen in Fig. 6a, 2EHN is positioned horizontally over the PEA subunit where there are weaker dispersion forces between its alkyl chain and that of PEA, whereas HPN forms one hydrogen bond with the carbonyl group on the PEA (Fig. 6b). This is consistent with binding energies of 11.8 kcal mol^{-1} and 13.5 kcal mol^{-1} for 2EHN and HPN, respectively. For HPN to be taken up, the HPN molecule must find a carbonyl with which to form a hydrogen bond, which introduces a steric component to the uptake. The interaction of 2EHN with the surface through dispersion interactions is less sterically demanding. Thus, although the binding energy for 2EHN is smaller, the higher net uptake coefficient for 2EHN is consistent with the lack of a significant steric effect. Like HPN, HHN is also able to form a hydrogen bond with PEA to anchor it to the substrate molecule (Fig. 6c) with a binding energy of 14.5 kcal mol^{-1}, and prefers to orient itself vertically with the carbon tail away from the PEA.

Further insight was gained by carrying out calculations for two nitrate molecules interacting with the PEA subunit. Fig. S9† shows the optimized structures. The binding energies for these structures are also found in Table S3.† The binding energies for 2EHN and HPN are similar (18.0 and 18.5 kcal mol^{-1}, respectively) and higher than for one organic nitrate on one PEA subunit. The binding energy for two HHN molecules with one PEA subunit is much higher, 30.0 kcal mol^{-1}. This is due to a contribution from hydrogen bonding between the HHN nitrate functional group and the PEA terminal hydroxyl group. Since only one PEA subunit was used to represent the substrate, and the polymer itself does not have repeating internal hydroxyl groups, the importance of binding to the terminal hydroxyl and the binding energies may be overestimated. However, the structure in Fig. S9c† shows both HHN molecules assemble vertically, indicating the HHN molecules may be able to assemble along the surface of PEA similar to a self-assembled monolayer, allowing for some dispersive interactions between the HHN carbon backbones.

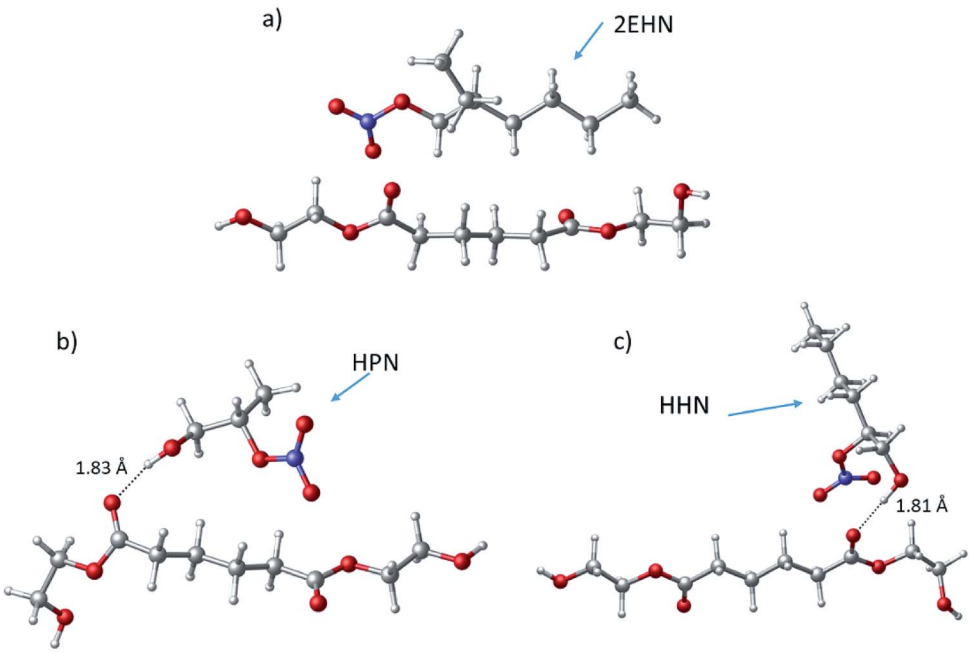

Fig. 6 The optimized structure for (a) one 2EHN molecule binding to one PEA subunit, (b) one HPN molecule binding to one PEA subunit, and (c) one HHN molecule binding to one PEA subunit. Hydrogen bonds are labeled with their bond length and bond angle.

Table 3 Average mole ratios[a] of $-ONO_2$ to $-C{=}O$ for PA, PEA, and SOA after exposure to each organic nitrate for 1047 seconds where equilibrium has been reached

Nitrates	Substrates	Mole ratio[a]
HHN	SOA	0.36 ± 0.06
	PA	0.59 ± 0.16
	PEA	0.12 ± 0.04
HPN	SOA	0.55 ± 0.29
	PA	0.27 ± 0.12
	PEA	0.077 ± 0.031
2EHN	SOA	0.088 ± 0.007
	PA	0.24 ± 0.12
	PEA	0.046 ± 0.006

[a] Error bars are $\pm 1\sigma$ from the average of multiple experiments.

Partition coefficients and mole ratios of organic nitrates

From the plateau region of Fig. 4, mole ratios were calculated for each organic nitrate-substrate combination. Table 3 shows the average ratio of moles of $-ONO_2$ to moles of $C{=}O$ after exposing SOA, PA and PEA to each organic nitrate for ~1000 seconds. The mole ratios show large amounts of organic nitrate, up to 0.59 for the case of HHN on PA. These large ratios of nitrate to substrate suggest that the nitrate is not simply adsorbing onto the surface of the solid films, but is penetrating and diffusing into the films as discussed above.

Partition coefficients (K) were calculated as described above (eqn (4)) and are summarized in Table 2 and Fig. 7. As shown in Fig. 7, HHN has the largest partition coefficient (*i.e.*, the largest solubility), with values up to two orders of magnitude larger than the other organic nitrates. Additionally, the K values for HHN exhibit a clear trend across the substrates, with $K^{SOA} \sim K^{PA} > K^{PEA}$. This same trend also holds for the K values of HPN, while for 2EHN $K^{PA} > K^{SOA} \gtrsim K^{PEA}$.

While 2EHN and HPN both exhibit a decrease in partition coefficient from PA to PEA and an increase from PEA to SOA, the relative magnitude of the partition coefficients changes. For example, while for PA the values are within experimental error of each other, for SOA, $K^{2EHN} < K^{HPN}$. The differences in their intermolecular interactions provide some insight into these trends. In the case of HPN, H-bonding will dominate as it can both donate and accept H-bonds. In contrast, dispersion forces will dominate for 2EHN with its larger alkyl chain. The crystal structure of PA exhibits a head-to-tail arrangement, with the acidic hydrogen of one molecule hydrogen bonding to the ketone carbonyl of the next molecule.[139] Although the PA in the film may no longer be in the crystalline form, the FTIR spectrum for the PA film indicates the carbonyl-containing groups are hydrogen-bonded (Fig. S5†), which is similar to the crystal structure. The acid carbonyl does not participate in the self-hydrogen bonding network, and therefore can accept hydrogen bonds from other molecules, for example from HPN. However, PA also has a significant hydrocarbon backbone, allowing the dispersion forces to contribute as well. The relative strength of these interactions are apparently similar enough to cause 2EHN and HPN to have similar solubilities in PA.

For SOA, the partition coefficient for HPN is about a factor of two larger than for 2EHN, indicating stronger attractive forces between the components of SOA and HPN. SOA is an amorphous mixture containing many different acids and polar functionalities that are available to hydrogen bond to the –OH group of HPN as well as its $-ONO_2$ group.[108] The additional hydrogen-bonding capacity of HPN appears to play a significant role in enhancing its solubility in SOA compared to the solubility of 2EHN.

It is important to note that vapor pressures are not necessarily a good measure of incorporation of the nitrates into the organic substrates. Thus while 2EHN and HPN have similar vapor pressures (Table 1), the solubility of HPN in SOA is double

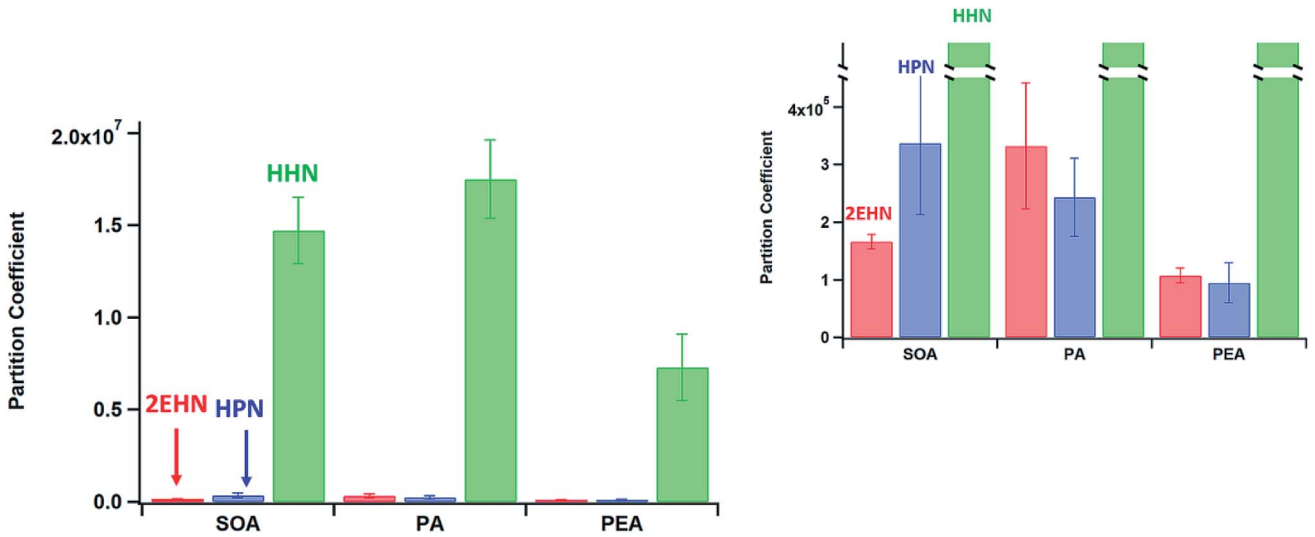

Fig. 7 Equilibrium partition coefficients for the organic nitrates into SOA, PA, and PEA. The inset is rescaled to show 2EHN and HPN. Error bars are the statistical $\pm 1\sigma$ from the average of multiple experiments for each nitrate.

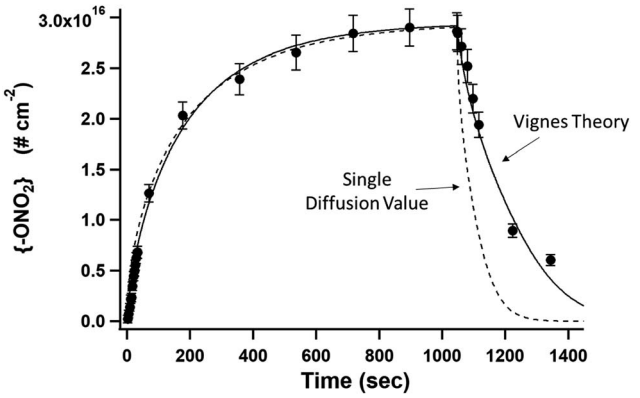

Fig. 8 Uptake of HHN on PA. Points are the experimental data, where the error bars represent the uncertainty in the nitrate absorption cross section ($\pm 2\sigma$). The solid line shows the prediction from KM-GAP using a changing composition-dependent diffusion coefficient scenario with Vignes equations, while the dashed line shows the prediction using a constant composition-independent diffusion coefficient.

that of 2EHN. Similarly, the net uptake coefficient of HPN on PEA is about a third of that for 2EHN.

Likewise, the O : C ratio (see ESI,† Section 3) is not a good predictor of uptake and partitioning. The O : C ratios for PEA and SOA are similar, 0.52 and 0.50, respectively. However the partition coefficients for all of the organic nitrates are greater on SOA than on PEA. The O : C for PA is smaller (0.30), yet the partition coefficient of HHN is higher than in PEA and perhaps SOA. Similarly, the solubility of 2EHN and HPN are relatively large for PA relative to the PEA and SOA. Additionally, while the O : C ratio for PA is smaller than that of SOA and PEA, the uptake coefficients are similar across all three substrates. This emphasizes the importance of understanding intermolecular interactions both at the surface and in the bulk as fundamental to the process of SOA growth in the atmosphere.

The relative values of the partition coefficients for 2EHN and HHN, which have similar chain lengths but different functional groups, agrees well with air–octanol partition coefficients for some organic nitrates reported by Treves *et al.*[140] Their coefficients showed that the addition of the hydroxyl group increased the solubility of the organic nitrates by over two orders of magnitude when compared to a C_5 alkyl nitrate, which is attributed to the increased hydrogen bonding capacity with the octanol. Additionally, when comparing different β-hydroxynitrates (such as HHN and HPN), the solubility in octanol was also enhanced as the length of the carbon chain increased.

KM-GAP

The KM-GAP model[136] was used to investigate diffusion of organic nitrates through the organic film into the bulk. One observation is that bulk diffusion coefficients need to be treated as composition-dependent with Vignes equations to reproduce the entire data set, and a composition-independent constant diffusion coefficient scenario did not accurately capture the

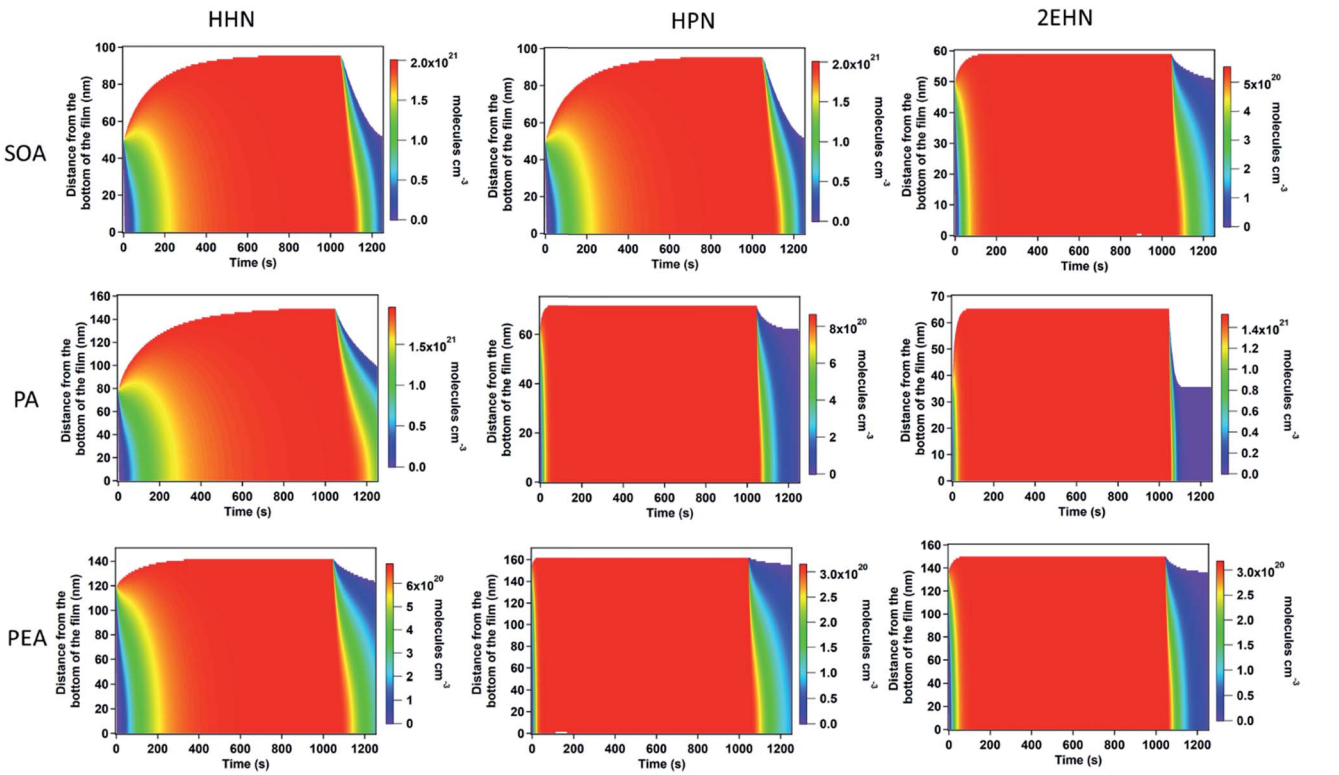

Fig. 9 Contour plots for the organic nitrate concentrations in molecules per cm^3 in the PA, PEA, and SOA films as a function of time and distance from the bottom of the film.

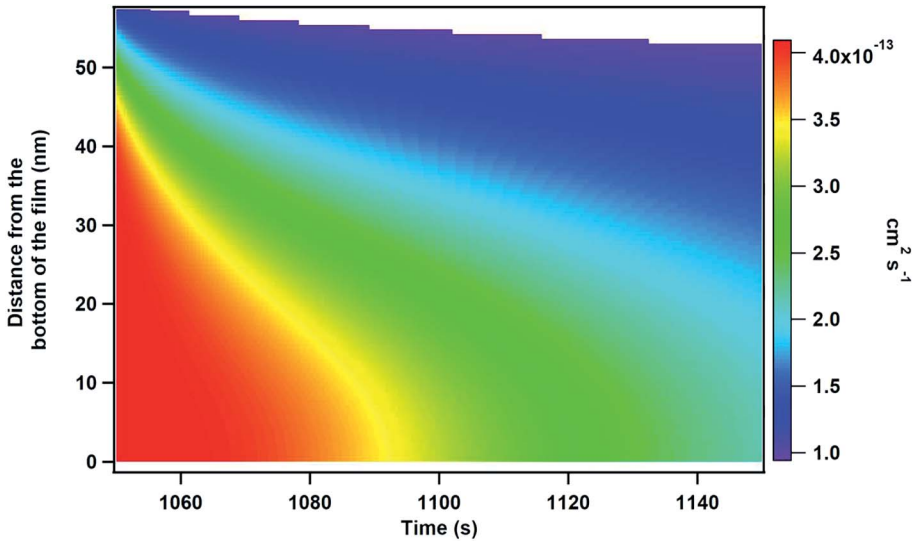

Fig. 10 An expanded view of the diffusion coefficient contour plot for 2EHN on SOA.

data set. An example is shown in Fig. 8 for uptake of HHN on PA. Although both parameterizations fit the uptake of the organic nitrate onto the substrate reasonably well, a constant diffusion coefficient over-predicted how quickly HHN would diffuse back out of the PA film, whereas a composition-dependent diffusion coefficient was a better match to the experimental data (Fig. 8, solid line). The parameters and coefficients used for the constant diffusion coefficient model are shown in Table S4.†

Fig. 9 shows the KM-GAP predicted concentration gradients for the organic nitrates as a function of time. The *y*-axis of Fig. 9 indicates the distance from the bottom of the film. These profiles indicate that the organic nitrate has indeed penetrated through the entirety of the film over the course of the experiments. Increases in the film thickness indicate that the organic film has swelled due to uptake of significant amounts of the organic nitrate. Fig. S10† shows the accompanying changes in diffusion coefficients predicted by the KM-GAP model. The profiles indicate that there is a plasticizing effect upon incorporation of the organic nitrate, shown by the increases in diffusion coefficients for several nitrate-substrate systems. Furthermore, upon desorption, the removal of the organic nitrate from the topmost layers of the substrate results in decreasing diffusion coefficients in the upper layers of the film as they partially re-solidify without the organic nitrate. This results in a 'crusting' scenario with higher diffusion coefficients (and thus lower viscosities) in the lower layers of the film and a more viscous outer layer or 'crust' towards the surface. Fig. 10 shows an expanded view as an example of the crusting on the surface of the film of SOA as 2EHN desorbs from the surface layer. This 'crusting' effect has been observed in previous work by Boyd *et al.*[141] on the evaporation kinetics of mixed limonene and β-pinene SOA, as well as by Pfrang *et al.*[142] on the chemical aging and transformation of multi-component organic aerosol particles.

Comparison of trends in uptake coefficients and partitioning

HHN exhibits the largest partition and net uptake coefficients compared to the other organic nitrates, and also provides the

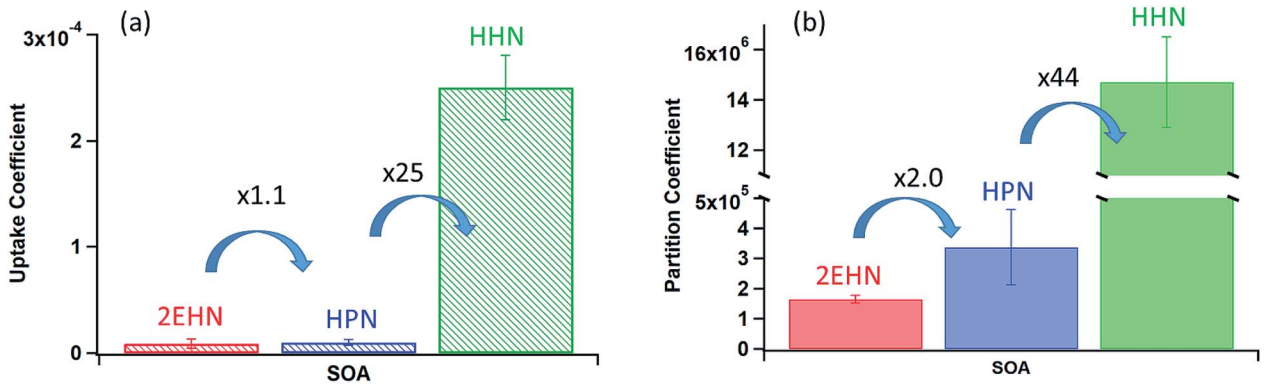

Fig. 11 (a) Initial uptake coefficients and (b) equilibrium partition coefficients for all organic nitrates into SOA. Error bars are $\pm 1\sigma$ from the average of multiple experiments for each organic nitrate.

most pronounced differences in uptake *versus* solubility across the three substrates. The uptake coefficient for HHN is similar for SOA, PA and PEA (Fig. 5 and Table 2), while the solubility of HHN in PEA is lower than that in PA and SOA (Fig. 7 and Table 2). This suggests that the interactions between the nitrate and the substrate in the bulk are different than those controlling uptake at the substrate surface.

Fig. 11 compares the trends in net uptake and partition coefficients for the three nitrates on SOA. While the uptake coefficient increases by a factor of 28 from 2EHN to HHN, the partition coefficient increases by a factor of 88. Thus, the solubility increases relatively more than the uptake coefficient, indicating that the relative contributions of the different attractive forces between the organic nitrates and the substrate must differ for the surface relative to those in the bulk. This is intuitively reasonable, given that the organic nitrates in the bulk are surrounded by neighboring molecules with opportunities to optimize the full range of van der Waals' interactions, including H-bonding, electrostatic interactions between partial charges, and dispersion interactions. On the other hand, an incoming gaseous organic nitrate molecule is affected only by available functional groups located on the surface, which will determine the nature and magnitude of the attractive forces. In the case of HHN on SOA, for example, if HHN is H-bonded to the surface in such a manner that the interactions of the alkyl chain with the surface are less than in the bulk where the HHN is engulfed by SOA components, relatively smaller uptake coefficients than expected based on the bulk behavior could result. Consistent with this, Fig. 6c shows that HHN is predicted to be oriented perpendicular to the PEA surface, minimizing dispersion forces between HHN and the surface PEA. This illustrates the importance of understanding both the nature of the surface and the nature of the gas in predicting uptake of gases into highly viscous particles, and hence their growth mechanisms in air.

Conclusions

Intermolecular interactions between gases and atmospheric particle surfaces play an important role in SOA particle growth. The present results indicate that a combination of polar and nonpolar interactions with the surface of SOA particles formed by the ozonolysis of α-pinene play a role in gas uptake. However, the interactions determining this uptake are not necessarily the same as those occurring in the bulk, and hence the uptake coefficients and partition coefficients do not always correlate. Trends in vapor pressure and O : C ratio are also not necessarily good indicators of uptake or partitioning. Note that these uptake coefficients may be orders of magnitude less than one and will certainly depend on both the nature of the gas and surface. Gas partitioning into these substrates has the ability to change the viscosity of the film and thus to increase the diffusion coefficients in the bulk. Furthermore, diffusion coefficients can decrease as the nitrates diffuse back out due to the formation of a crust near the surface. This has implications in the kinetics of condensed phase chemistry occurring in the bulk *versus* at the surface of particles. More knowledge of the nature of the surface of SOA particles, and how gaseous species interact with these surfaces, will allow for a better understanding of SOA particle growth to better predict their effects on Earth's climate.

Conflicts of interest

There are no conflicts to declare.

Acknowledgements

This work was funded by the NSF (Grant # 1647386), by the NSF Major Research Instrumentation (MRI) program (Grants #1337080 and #0923323), and the Army Research Office (Grant #W911NF1710105). M. S. acknowledges funding from NSF (CAREER, AGS-1654104) and M. S. and P. L. thank T. Berkemeier for sharing the code of MCGA. The authors thank the University of California Irvine NMR Facility and Cambustion, Ltd. (Cambridge, UK) for loan of the aerodynamic aerosol classifier.

References

1 B. J. Finlayson-Pitts and J. N. Pitts, *Chemistry of the Upper and Lower Atmosphere: Theory, Experiments, and Applications*, Academic Press, 2000.
2 J. H. Seinfeld and S. N. Pandis, *Atmospheric Chemistry and Physics: From Air Pollution to Climate Change*, Wiley, 2006.
3 W. C. Hinds, *Aerosol Technology: Properties, Behavior, and Measurement of Airborne Particles*, John Wiley & Sons, 1982.
4 A. Singh, W. J. Bloss and F. D. Pope, 60 years of UK visibility measurements: impact of meteorology and atmospheric pollutants on visibility, *Atmos. Chem. Phys.*, 2017, **17**, 2085–2101.
5 U. Pöschl and M. Shiraiwa, Multiphase chemistry at the atmosphere–biosphere interface influencing climate and public health in the anthropocene, *Chem. Rev.*, 2015, **115**, 4440–4475.
6 C. A. Pope and D. W. Dockery, Health effects of fine particulate air pollution: lines that connect, *J. Air Waste Manage. Assoc.*, 2006, **56**, 709–742.
7 J. L. Mauderly and J. C. Chow, Health effects of organic aerosols, *Inhalation Toxicol.*, 2008, **20**, 257–288.
8 M. R. Heal, P. Kumar and R. M. Harrison, Particles, air quality, policy and health, *Chem. Soc. Rev.*, 2012, **41**, 6606–6630.
9 A. Nel, Air pollution-related illness: effects of particles, *Science*, 2005, **308**, 804–806.
10 G. B. Hamra, N. Guha, A. Cohen, F. Laden, O. Raaschou-Nielsen, J. M. Samet, P. Vineis, F. Forastiere, P. Saldiva, T. Yorifuji and D. Loomis, Outdoor particulate matter exposure and lung cancer: a systematic review and meta-analysis, *Environ. Health Perspect.*, 2014, **122**, 906–911.
11 P. M. Mannucci, S. Harari, I. Martinelli and M. Franchini, Effects on health of air pollution: a narrative review, *Intern. Emerg. Med.*, 2015, **10**, 657–662.
12 R. E. Wyzga and A. C. Rohr, Long-term particulate matter exposure: attributing health effects to individual PM components, *J. Air Waste Manage. Assoc.*, 2015, **65**, 523–543.

13 J. Lelieveld, J. S. Evans, M. Fnais, D. Giannadaki and A. Pozzer, The contribution of outdoor air pollution sources to premature mortality on a global scale, *Nature*, 2015, **525**, 367–374.

14 P. J. Landrigan, R. Fuller, N. J. R. Acosta, O. Adeyi, R. Arnold, N. Basu, A. B. Baldé, R. Bertollini, S. Bose-O'Reilly, J. I. Boufford, P. N. Breysse, T. Chiles, C. Mahidol, A. M. Coll-Seck, M. L. Cropper, J. Fobil, V. Fuster, M. Greenstone, A. Haines, D. Hanrahan, D. Hunter, M. Khare, A. Krupnick, B. Lanphear, B. Lohani, K. Martin, K. V. Mathiasen, M. A. McTeer, C. J. L. Murray, J. D. Ndahimananjara, F. Perera, J. Potočnik, A. S. Preker, J. Ramesh, J. Rockström, C. Salinas, L. D. Samson, K. Sandilya, P. D. Sly, K. R. Smith, A. Steiner, R. B. Stewart, W. A. Suk, O. C. P. van Schayck, G. N. Yadama, K. Yumkella and M. Zhong, The Lancet Commission on pollution and health, *Lancet*, 2018, **391**, 462–512.

15 O. Boucher, D. Randall, P. Artaxo, C. Bretherton, G. Feingold, P. Forster, V.-M. Kerminen, Y. Kondo, H. Liao, U. Lohmann, P. Rasch, S. K. Satheesh, S. Sherwood, B. Stevens and X. Y. Zhang, Clouds and Aerosols, in *Climate Change 2013: The Physical Science Basis. Contribution of Working Group I to the Fifth Assessment Report of the Intergovernmental Panel on Climate Change*, ed. T. F. Stocker, D. Qin, G.-K. Plattner, M. Tignor, S. K. Allen, J. Boschung, A. Nauels, Y. Xia, V. Bex and P. M. Midgley, Cambridge University Press, Cambridge, United Kingdom and New York, NY, USA, 2013, DOI: 10.1017/cbo9781107415324.

16 R. F. Phalen, *Inhalation studies: Foundation and techniques*, Informa Healthcare, 2009.

17 M. Kanakidou, J. H. Seinfeld, S. N. Pandis, I. Barnes, F. J. Dentener, M. C. Facchini, R. Van Dingenen, B. Ervens, A. Nenes, C. J. Nielsen, E. Swietlicki, J. P. Putaud, Y. Balkanski, S. Fuzzi, J. Horth, G. K. Moortgat, R. Winterhalter, C. E. L. Myhre, K. Tsigaridis, E. Vignati, E. G. Stephanou and J. Wilson, Organic aerosol and global climate modelling: a review, *Atmos. Chem. Phys.*, 2005, **5**, 1053–1123.

18 S. Fuzzi, M. O. Andreae, B. J. Huebert, M. Kulmala, T. C. Bond, M. Boy, S. J. Doherty, A. Guenther, M. Kanakidou, K. Kawamura, V. M. Kerminen, U. Lohmann, L. M. Russell and U. Pöschl, Critical assessment of the current state of scientific knowledge, terminology, and research needs concerning the role of organic aerosols in the atmosphere, climate, and global change, *Atmos. Chem. Phys.*, 2006, **6**, 2017–2038.

19 M. Hallquist, J. C. Wenger, U. Baltensperger, Y. Rudich, D. Simpson, M. Claeys, J. Dommen, N. M. Donahue, C. George, A. H. Goldstein, J. F. Hamilton, H. Herrmann, T. Hoffmann, Y. Iinuma, M. Jang, M. E. Jenkin, J. L. Jimenez, A. Kiendler-Scharr, W. Maenhaut, G. McFiggans, T. F. Mentel, A. Monod, A. S. H. Prevot, J. H. Seinfeld, J. D. Surratt, R. Szmigielski and J. Wildt, The formation, properties and impact of secondary organic aerosol: current and emerging issues, *Atmos. Chem. Phys.*, 2009, **9**, 5155–5236.

20 J. P. D. Abbatt, A. K. Y. Lee and J. A. Thornton, Quantifying trace gas uptake to tropospheric aerosol: recent advances and remaining challenges, *Chem. Soc. Rev.*, 2012, **41**, 6555–6581.

21 R. Y. Zhang, G. H. Wang, S. Guo, M. L. Zarnora, Q. Ying, Y. Lin, W. G. Wang, M. Hu and Y. Wang, Formation of urban fine particulate matter, *Chem. Rev.*, 2015, **115**, 3803–3855.

22 R. Y. Zhang, A. Khalizov, L. Wang, M. Hu and W. Xu, Nucleation and growth of nanoparticles in the atmosphere, *Chem. Rev.*, 2012, **112**, 1957–2011.

23 C. E. Kolb, R. A. Cox, J. P. D. Abbatt, M. Ammann, E. J. Davis, D. J. Donaldson, B. C. Garrett, C. George, P. T. Griffiths, D. R. Hanson, M. Kulmala, G. McFiggans, U. Pöschl, I. Riipinen, M. J. Rossi, Y. Rudich, P. E. Wagner, P. M. Winkler, D. R. Worsnop and C. D. O' Dowd, An overview of current issues in the uptake of atmospheric trace gases by aerosols and clouds, *Atmos. Chem. Phys.*, 2010, **10**, 10561–10605.

24 I. Riipinen, T. Yli-Juuti, J. R. Pierce, T. Petäjä, D. R. Worsnop, M. Kulmala and N. M. Donahue, The contribution of organics to atmospheric nanoparticle growth, *Nat. Geosci.*, 2012, **5**, 453.

25 M. Shrivastava, C. D. Cappa, J. Fan, A. H. Goldstein, A. B. Guenther, J. L. Jimenez, C. Kuang, A. Laskin, S. T. Martin, N. L. Ng, T. Petäjä, J. R. Pierce, P. J. Rasch, P. Roldin, J. H. Seinfeld, J. Shilling, J. N. Smith, J. A. Thornton, R. Volkamer, J. Wang, D. R. Worsnop, R. A. Zaveri, A. Zelenyuk and Q. Zhang, Recent advances in understanding secondary organic aerosol: implications for global climate forcing, *Rev. Geophys.*, 2017, **55**, 509–559.

26 D. Stolzenburg, L. Fischer, A. L. Vogel, M. Heinritzi, M. Schervish, M. Simon, A. C. Wagner, L. Dada, L. R. Ahonen, A. Amorim, A. Baccarini, P. S. Bauer, B. Baumgartner, A. Bergen, F. Bianchi, M. Breitenlechner, S. Brilke, S. Buenrostro Mazon, D. Chen, A. Dias, D. C. Draper, J. Duplissy, I. El Haddad, H. Finkenzeller, C. Frege, C. Fuchs, O. Garmash, H. Gordon, X. He, J. Helm, V. Hofbauer, C. R. Hoyle, C. Kim, J. Kirkby, J. Kontkanen, A. Kürten, J. Lampilahti, M. Lawler, K. Lehtipalo, M. Leiminger, H. Mai, S. Mathot, B. Mentler, U. Molteni, W. Nie, T. Nieminen, J. B. Nowak, A. Ojdanic, A. Onnela, M. Passananti, T. Petäjä, L. L. J. Quéléver, M. P. Rissanen, N. Sarnela, S. Schallhart, C. Tauber, A. Tomé, R. Wagner, M. Wang, L. Weitz, D. Wimmer, M. Xiao, C. Yan, P. Ye, Q. Zha, U. Baltensperger, J. Curtius, J. Dommen, R. C. Flagan, M. Kulmala, J. N. Smith, D. R. Worsnop, A. Hansel, N. M. Donahue and P. M. Winkler, Rapid growth of organic aerosol nanoparticles over a wide tropospheric temperature range, *Proc. Natl. Acad. Sci. U. S. A.*, 2018, **115**, 9122–9127.

27 J. F. Pankow, Further discussion of the octanol/air partition coefficient K_{OA} as a correlating parameter for gas/particle partitioning coefficients, *Atmos. Environ.*, 1998, **32**, 1493–1497.

28 J. F. Pankow, An absorption model of gas/particle partitioning of organic compounds in the atmosphere, *Atmos. Environ.*, 1994, **28**, 185–188.

29 N. M. Donahue, I. K. Ortega, W. Chuang, I. Riipinen, F. Riccobono, S. Schobesberger, J. Dommen, U. Baltensperger, M. Kulmala, D. R. Worsnop and H. Vehkamaki, How do organic vapors contribute to new-particle formation?, *Faraday Discuss.*, 2013, **165**, 91–104.

30 N. M. Donahue, A. L. Robinson, C. O. Stanier and S. N. Pandis, Coupled partitioning, dilution, and chemical aging of semivolatile organics, *Environ. Sci. Technol.*, 2006, **40**, 2635–2643.

31 M. Shiraiwa and J. H. Seinfeld, Equilibration timescale of atmospheric secondary organic aerosol partitioning, *Geophys. Res. Lett.*, 2012, **39**, L24801, DOI: 24810.21029/22012gl054008.

32 J. P. Reid, A. K. Bertram, D. O. Topping, A. Laskin, S. T. Martin, M. D. Petters, F. D. Pope and G. Rovelli, The viscosity of atmospherically relevant organic particles, *Nat. Commun.*, 2018, **9**, 956, DOI: 910.1038/s41467-41018-03027-z.

33 T. D. Vaden, D. Imre, J. Beránek, M. Shrivastava and A. Zelenyuk, Evaporation kinetics and phase of laboratory and ambient secondary organic aerosol, *Proc. Natl. Acad. Sci. U. S. A.*, 2011, **108**, 2190–2195.

34 A. Virtanen, J. Kannosto, H. Kuuluvainen, A. Arffman, J. Joutsensaari, E. Saukko, L. Hao, P. Yli-Pirila, P. Tiitta, J. K. Holopainen, J. Keskinen, D. R. Worsnop, J. N. Smith and A. Laaksonen, Bounce behavior of freshly nucleated biogenic secondary organic aerosol particles, *Atmos. Chem. Phys.*, 2011, **11**, 8759–8766.

35 L. Renbaum-Wolff, J. W. Grayson, A. P. Bateman, M. Kuwata, M. Sellier, B. J. Murray, J. E. Shilling, S. T. Martin and A. K. Bertram, Viscosity of alpha-pinene secondary organic material and implications for particle growth and reactivity, *Proc. Natl. Acad. Sci. U. S. A.*, 2013, **110**, 8014–8019.

36 T. Koop, J. Bookhold, M. Shiraiwa and U. Pöschl, Glass transition and phase state of organic compounds: dependency on molecular properties and implications for secondary organic aerosols in the atmosphere, *Phys. Chem. Chem. Phys.*, 2011, **13**, 19238–19255.

37 S. M. Zhou, M. Shiraiwa, R. D. McWhinney, U. Pöschl and J. P. D. Abbatt, Kinetic limitations in gas–particle reactions arising from slow diffusion in secondary organic aerosol, *Faraday Discuss.*, 2013, **165**, 391–406.

38 C. Kidd, V. Perraud, L. M. Wingen and B. J. Finlayson-Pitts, Integrating phase and composition of secondary organic aerosol from the ozonolysis of alpha-pinene, *Proc. Natl. Acad. Sci. U. S. A.*, 2014, **111**, 7552–7557.

39 V. Perraud, E. A. Bruns, M. J. Ezell, S. N. Johnson, Y. Yu, M. L. Alexander, A. Zelenyuk, D. Imre, W. L. Chang, D. Dabdub, J. F. Pankow and B. J. Finlayson-Pitts, Nonequilibrium atmospheric secondary organic aerosol formation and growth, *Proc. Natl. Acad. Sci. U. S. A.*, 2012, **109**, 2836–2841.

40 A. Virtanen, J. Joutsensaari, T. Koop, J. Kannosto, P. Yli-Pirila, J. Leskinen, J. M. Makela, J. K. Holopainen, U. Pöschl, M. Kulmala, D. R. Worsnop and A. Laaksonen, An amorphous solid state of biogenic secondary organic aerosol particles, *Nature*, 2010, **467**, 824–827.

41 M. Shiraiwa, M. Ammann, T. Koop and U. Pöschl, Gas uptake and chemical aging of semisolid organic aerosol particles, *Proc. Natl. Acad. Sci. U. S. A.*, 2011, **108**, 11003–11008.

42 C. D. Cappa and K. R. Wilson, Evolution of organic aerosol mass spectra upon heating: implications for OA phase and partitioning behavior, *Atmos. Chem. Phys.*, 2011, **11**, 1895–1911.

43 P. J. Ziemann, Phase matters for aerosols, *Nature*, 2010, **467**, 797–798.

44 F. H. Marshall, R. E. H. Miles, Y. C. Song, P. B. Ohm, R. M. Power, J. P. Reid and C. S. Dutcher, Diffusion and reactivity in ultraviscous aerosol and the correlation with particle viscosity, *Chem. Sci.*, 2016, **7**, 1298–1308.

45 N. A. Hosny, C. Fitzgerald, C. Tong, M. Kalberer, M. K. Kuimova and F. D. Pope, Fluorescent lifetime imaging of atmospheric aerosols: a direct probe of aerosol viscosity, *Faraday Discuss.*, 2013, **165**, 343–356.

46 N. A. Hosny, C. Fitzgerald, A. Vyšniauskas, A. Athanasiadis, T. Berkemeier, N. Uygur, U. Pöschl, M. Shiraiwa, M. Kalberer, F. D. Pope and M. K. Kuimova, Direct imaging of changes in aerosol particle viscosity upon hydration and chemical aging, *Chem. Sci.*, 2016, **7**, 1357–1367.

47 Y. Zhang, M. S. Sanchez, C. Douet, Y. Wang, A. P. Bateman, Z. Gong, M. Kuwata, L. Renbaum-Wolff, B. B. Sato, P. F. Liu, A. K. Bertram, F. M. Geiger and S. T. Martin, Changing shapes and implied viscosities of suspended submicron particles, *Atmos. Chem. Phys.*, 2015, **15**, 7819–7829.

48 A. Pajunoja, J. Malila, L. Hao, J. Joutsensaari, K. E. J. Lehtinen and A. Virtanen, Estimating the viscosity range of SOA particles based on their coalescence time, *Aerosol Sci. Technol.*, 2014, **48**, i–iv.

49 A. Pajunoja, A. T. Lambe, J. Hakala, N. Rastak, M. J. Cummings, J. F. Brogan, L. Hao, M. Paramonov, J. Hong, N. L. Prisle, J. Malila, S. Romakkaniemi, K. E. J. Lehtinen, A. Laaksonen, M. Kulmala, P. Massoli, T. B. Onasch, N. M. Donahue, I. Riipinen, P. Davidovits, D. R. Worsnop, T. Petäjä and A. Virtanen, Adsorptive uptake of water by semisolid secondary organic aerosols, *Geophys. Res. Lett.*, 2015, **42**, 3063–3068.

50 H. Mai, M. Shiraiwa, R. C. Flagan and J. H. Seinfeld, Under what conditions can equilibrium gas–particle partitioning be expected to hold in the atmosphere?, *Environ. Sci. Technol.*, 2015, **49**, 11485–11491.

51 L. I. Kleinman, S. R. Springston, J. Wang, P. H. Daum, Y. N. Lee, L. J. Nunnermacker, G. I. Senum, J. Weinstein-Lloyd, M. L. Alexander, J. Hubbe, J. Ortega, R. A. Zaveri, M. R. Canagaratna and J. Jayne, The time evolution of aerosol size distribution over the Mexico City plateau, *Atmos. Chem. Phys.*, 2009, **9**, 4261–4278.

52 F. Yu, A secondary organic aerosol formation model considering successive oxidation aging and kinetic condensation of organic compounds: global scale implications, *Atmos. Chem. Phys.*, 2011, **11**, 1083–1099.

53 K. Dzepina, R. M. Volkamer, S. Madronich, P. Tulet, I. M. Ulbrich, Q. Zhang, C. D. Cappa, P. J. Ziemann and

J. L. Jimenez, Evaluation of recently-proposed secondary organic aerosol models for a case study in Mexico City, *Atmos. Chem. Phys.*, 2009, **9**, 5681–5709.

54 C. D. Cappa and J. L. Jimenez, Quantitative estimates of the volatility of ambient organic aerosol, *Atmos. Chem. Phys.*, 2010, **10**, 5409–5424.

55 X. Zhang, S. N. Pandis and J. H. Seinfeld, Diffusion-limited *versus* quasi-equilibrium aerosol growth, *Aerosol Sci. Technol.*, 2012, **46**, 874–885.

56 M. Shiraiwa, Y. Li, A. P. Tsimpidi, V. A. Karydis, T. Berkemeier, S. N. Pandis, J. Lelieveld, T. Koop and U. Pöschl, Global distribution of particle phase state in atmospheric secondary organic aerosols, *Nat. Commun.*, 2017, **8**, 15002, DOI: 15010.11038/ncomms15002.

57 R. A. Zaveri, J. E. Shilling, A. Zelenyuk, J. Liu, D. M. Bell, E. L. D'Ambro, C. J. Gaston, J. A. Thornton, A. Laskin, P. Lin, J. Wilson, R. C. Easter, J. Wang, A. K. Bertram, S. T. Martin, J. H. Seinfeld and D. R. Worsnop, Growth kinetics and size distribution dynamics of viscous secondary organic aerosol, *Environ. Sci. Technol.*, 2018, **52**, 1191–1199.

58 C. Wang, F. Wania and K.-U. Goss, Is secondary organic aerosol yield governed by kinetic factors rather than equilibrium partitioning?, *Environ. Sci.: Processes Impacts*, 2018, **20**, 245–252.

59 Z. Gong, Y. Han, P. Liu, J. Ye, F. N. Keutsch, K. A. McKinney and S. T. Martin, Influence of particle physical state on the uptake of medium-sized organic molecules, *Environ. Sci. Technol.*, 2018, **52**, 8381–8389.

60 A. Zelenyuk, D. G. Imre, J. Wilson, D. M. Bell, K. J. Suski, M. Shrivastava, J. Beránek, M. L. Alexander, A. L. Kramer and S. L. Massey Simonich, The effect of gas-phase polycyclic aromatic hydrocarbons on the formation and properties of biogenic secondary organic aerosol particles, *Faraday Discuss.*, 2017, **200**, 143–164.

61 A. Zelenyuk, D. Imre, J. Beránek, E. Abramson, J. Wilson and M. Shrivastava, Synergy between secondary organic aerosols and long-range transport of polycyclic aromatic hydrocarbons, *Environ. Sci. Technol.*, 2012, **46**, 12459–12466.

62 E. Abramson, D. Imre, J. Beránek, J. Wilson and A. Zelenyuk, Experimental determination of chemical diffusion within secondary organic aerosol particles, *Phys. Chem. Chem. Phys.*, 2013, **15**, 2983–2991.

63 B. Zobrist, V. Soonsin, B. P. Luo, U. K. Krieger, C. Marcolli, T. Peter and T. Koop, Ultra-slow water diffusion in aqueous sucrose glasses, *Phys. Chem. Chem. Phys.*, 2011, **13**, 3514–3526.

64 D. M. Lienhard, A. J. Huisman, U. K. Krieger, Y. Rudich, C. Marcolli, B. Luo, D. L. Bones, J. P. Reid, A. T. Lambe and M. R. Canagaratna, Viscous organic aerosol particles in the upper troposphere: diffusivity-controlled water uptake and ice nucleation?, *Atmos. Chem. Phys.*, 2015, **15**, 13599–13613.

65 H. J. Tong, J. P. Reid, D. L. Bones, B. P. Luo and U. K. Krieger, Measurements of the timescales for the mass transfer of water in glassy aerosol at low relative humidity and ambient temperature, *Atmos. Chem. Phys.*, 2011, **11**, 4739–4754.

66 D. L. Bones, J. P. Reid, D. M. Lienhard and U. K. Krieger, Comparing the mechanism of water condensation and evaporation in glassy aerosol, *Proc. Natl. Acad. Sci. U. S. A.*, 2012, **109**, 11613–11618.

67 T. Berkemeier, S. S. Steimer, U. K. Krieger, T. Peter, U. Pöschl, M. Ammann and M. Shiraiwa, Ozone uptake on glassy, semi-solid and liquid organic matter and the role of reactive oxygen intermediates in atmospheric aerosol chemistry, *Phys. Chem. Chem. Phys.*, 2016, **18**, 12662–12674.

68 S. Zhou, M. Shiraiwa, R. D. McWhinney, U. Pöschl and J. P. D. Abbatt, Kinetic limitations in gas–particle reactions arising from slow diffusion in secondary organic aerosol, *Faraday Discuss.*, 2013, **165**, 391–406.

69 N. O. A. Kwamena, M. G. Staikova, D. J. Donaldson, I. J. George and J. P. D. Abbatt, Role of the aerosol substrate in the heterogeneous ozonation reactions of surface-bound PAHs, *J. Phys. Chem. A*, 2007, **111**, 11050–11058.

70 L. Lee and K. Wilson, The reactive–diffusive length of OH and ozone in model organic aerosols, *J. Phys. Chem. A*, 2016, **120**, 6800–6812.

71 J. H. Slade and D. A. Knopf, Multiphase OH oxidation kinetics of organic aerosol: the role of particle phase state and relative humidity, *Geophys. Res. Lett.*, 2014, **41**, 5297–5306.

72 A. M. Arangio, J. H. Slade, T. Berkemeier, U. Pöschl, D. A. Knopf and M. Shiraiwa, Multiphase chemical kinetics of OH radical uptake by molecular organic markers of biomass burning aerosols: humidity and temperature dependence, surface reaction, and bulk diffusion, *J. Phys. Chem. A*, 2015, **119**, 4533–4544.

73 M. Shiraiwa, U. Pöschl and D. A. Knopf, Multiphase chemical kinetics of NO_3 radicals reacting with organic aerosol components from biomass burning, *Environ. Sci. Technol.*, 2012, **46**, 6630–6636.

74 P. S. J. Lakey, T. Berkemeier, M. Krapf, J. Dommen, S. S. Steimer, L. K. Whalley, T. Ingham, M. T. Baeza-Romero, U. Pöschl, M. Shiraiwa, M. Ammann and D. E. Heard, The effect of viscosity and diffusion on the HO_2 uptake by sucrose and secondary organic aerosol particles, *Atmos. Chem. Phys.*, 2016, **16**, 13035–13047.

75 M. Kuwata and S. T. Martin, Phase of atmospheric secondary organic material affects its reactivity, *Proc. Natl. Acad. Sci. U. S. A.*, 2012, **109**, 17354–17359.

76 D. M. Bell, D. Imre, S. T. Martin and A. Zelenyuk, The properties and behavior of α-pinene secondary organic aerosol particles exposed to ammonia under dry conditions, *Phys. Chem. Chem. Phys.*, 2017, **19**, 6497–6507.

77 Y. J. Li, P. Liu, Z. Gong, Y. Wang, A. P. Bateman, C. Bergoend, A. K. Bertram and S. T. Martin, Chemical reactivity and liquid/nonliquid states of secondary organic material, *Environ. Sci. Technol.*, 2015, **49**, 13264–13274.

78 M. C. Fairhurst, M. J. Ezell, C. Kidd, P. S. J. Lakey, M. Shiraiwa and B. J. Finlayson-Pitts, Kinetics,

mechanisms and ionic liquids in the uptake of *n*-butylamine onto low molecular weight dicarboxylic acids, *Phys. Chem. Chem. Phys.*, 2017, **19**, 4827–4839.

79 M. C. Fairhurst, M. J. Ezell and B. J. Finlayson-Pitts, Knudsen cell studies of the uptake of gaseous ammonia and amines onto C_3–C_7 solid dicarboxylic acids, *Phys. Chem. Chem. Phys.*, 2017, **19**, 26296–26309.

80 X. Gao, Y. Zhang and Y. Liu, A kinetics study of the heterogeneous reaction of *n*-butylamine with succinic acid using an ATR-FTIR flow reactor, *Phys. Chem. Chem. Phys.*, 2018, **20**, 15464–15472.

81 L. P. Chan and C. K. Chan, Role of the aerosol phase state in ammonia/amines exchange reactions, *Environ. Sci. Technol.*, 2013, **47**, 5755–5762.

82 T. Berkemeier, A. J. Huisman, M. Ammann, M. Shiraiwa, T. Koop and U. Pöschl, Kinetic regimes and limiting cases of gas uptake and heterogeneous reactions in atmospheric aerosols and clouds: a general classification scheme, *Atmos. Chem. Phys.*, 2013, **13**, 6663–6686.

83 M. Ammann, U. Pöschl and Y. Rudich, Effects of reversible adsorption and Langmuir–Hinshelwood surface reactions on gas uptake by atmospheric particles, *Phys. Chem. Chem. Phys.*, 2003, **5**, 351–356.

84 M. Shiraiwa, C. Pfrang and U. Pöschl, Kinetic multi-layer model of aerosol surface and bulk chemistry (KM-SUB): the influence of interfacial transport and bulk diffusion on the oxidation of oleic acid by ozone, *Atmos. Chem. Phys.*, 2010, **10**, 3673–3691.

85 P. Roldin, A. C. Eriksson, E. Z. Nordin, E. Hermansson, D. Mogensen, A. Rusanen, M. Boy, E. Swietlicki, B. Svenningsson, A. Zelenyuk and J. Pagels, Modelling non-equilibrium secondary organic aerosol formation and evaporation with the aerosol dynamics, gas- and particle-phase chemistry kinetic multilayer model ADCHAM, *Atmos. Chem. Phys.*, 2014, **14**, 7953–7993.

86 U. Pöschl, Y. Rudich and M. Ammann, Kinetic model framework for aerosol and cloud surface chemistry and gas–particle interactions – Part 1: General equations, parameters, and terminology, *Atmos. Chem. Phys.*, 2007, **7**, 5989–6023.

87 A. Matsunaga and P. J. Ziemann, Yields of β-hydroxynitrates and dihydroxynitrates in aerosol formed from OH radical-initiated reactions of linear alkenes in the presence of NO_x, *J. Phys. Chem. A*, 2009, **113**, 599–606.

88 N. Sobanski, J. Thieser, J. Schuladen, C. Sauvage, W. Song, J. Williams, J. Lelieveld and J. N. Crowley, Day and night-time formation of organic nitrates at a forested mountain site in south-west Germany, Atmos, *Chem. Phys.*, 2017, **17**, 4115–4130.

89 R. Atkinson, S. M. Aschmann, W. P. Carter, A. M. Winer and J. N. Pitts Jr, Alkyl nitrate formation from the nitrogen oxide (NO_x)–air photooxidations of C_2–C_8 *n*-alkanes, *J. Phys. Chem.*, 1982, **86**, 4563–4569.

90 J. M. Roberts, The atmospheric chemistry of organic nitrates, *Atmos. Environ., Part A*, 1990, **24**, 243–287.

91 J. L. Fry, A. Kiendler-Scharr, A. W. Rollins, T. Brauers, S. S. Brown, H. P. Dorn, W. P. Dubé, H. Fuchs, A. Mensah, F. Rohrer, R. Tillmann, A. Wahner, P. J. Wooldridge and R. C. Cohen, SOA from limonene: role of NO_3 in its generation and degradation, *Atmos. Chem. Phys.*, 2011, **11**, 3879–3894.

92 M. Spittler, I. Barnes, I. Bejan, K. Brockmann, T. Benter and K. Wirtz, Reactions of NO_3 radicals with limonene and α-pinene: product and SOA formation, *Atmos. Environ.*, 2006, **40**, 116–127.

93 E. A. Bruns, V. Perraud, A. Zelenyuk, M. J. Ezell, S. N. Johnson, Y. Yu, D. Imre, B. J. Finlayson-Pitts and M. L. Alexander, Comparison of FTIR and particle mass spectrometry for the measurement of particulate organic nitrates, *Environ. Sci. Technol.*, 2010, **44**, 1056–1061.

94 R. Atkinson and J. Arey, Atmospheric degradation of volatile organic compounds, *Chem. Rev.*, 2003, **103**, 4605–4638.

95 J. L. Fry, D. C. Draper, K. C. Barsanti, J. N. Smith, J. Ortega, P. M. Winkler, M. J. Lawler, S. S. Brown, P. M. Edwards, R. C. Cohen and L. Lee, Secondary organic aerosol formation and organic nitrate yield from NO_3 oxidation of biogenic hydrocarbons, *Environ. Sci. Technol.*, 2014, **48**, 11944–11953.

96 N. L. Ng, S. S. Brown, A. T. Archibald, E. Atlas, R. C. Cohen, J. N. Crowley, D. A. Day, N. M. Donahue, J. L. Fry, H. Fuchs, R. J. Griffin, M. I. Guzman, H. Herrmann, A. Hodzic, Y. Iinuma, J. L. Jimenez, A. Kiendler-Scharr, B. H. Lee, D. J. Luecken, J. Mao, R. McLaren, A. Mutzel, H. D. Osthoff, B. Ouyang, B. Picquet-Varrault, U. Platt, H. O. T. Pye, Y. Rudich, R. H. Schwantes, M. Shiraiwa, J. Stutz, J. A. Thornton, A. Tilgner, B. J. Williams and R. A. Zaveri, Nitrate radicals and biogenic volatile organic compounds: oxidation, mechanisms, and organic aerosol, *Atmos. Chem. Phys.*, 2017, **17**, 2103–2162.

97 J. H. Slade, C. de Perre, L. Lee and P. B. Shepson, Nitrate radical oxidation of γ-terpinene: hydroxy nitrate, total organic nitrate, and secondary organic aerosol yields, *Atmos. Chem. Phys.*, 2017, **17**, 8635–8650.

98 C. Espada, J. Grossenbacher, K. Ford, T. Couch and P. B. Shepson, The production of organic nitrates from various anthropogenic volatile organic compounds, *Int. J. Chem. Kinet.*, 2005, **37**, 675–685.

99 A. W. Rollins, S. Pusede, P. Wooldridge, K. E. Min, D. R. Gentner, A. H. Goldstein, S. Liu, D. A. Day, L. M. Russell, C. L. Rubitschun, J. D. Surratt and R. C. Cohen, Gas/particle partitioning of total alkyl nitrates observed with TD-LIF in Bakersfield, *J. Geophys. Res.: Atmos.*, 2013, **118**, 6651–6662.

100 J. Kastler and K. Ballschmiter, Bifunctional alkyl nitrates – trace constituents of the atmosphere, *Fresenius. J. Anal. Chem.*, 1998, **360**, 812–816.

101 B. H. Lee, C. Mohr, F. D. Lopez-Hilfiker, A. Lutz, M. Hallquist, L. Lee, P. Romer, R. C. Cohen, S. Iyer, T. Kurten, W. W. Hu, D. A. Day, P. Campuzano-Jost, J. L. Jimenez, L. Xu, N. L. Ng, H. Y. Guo, R. J. Weber, R. J. Wild, S. S. Brown, A. Koss, J. de Gouw, K. Olson, A. H. Goldstein, R. Seco, S. Kim, K. McAvey, P. B. Shepson, T. Starn, K. Baumann, E. S. Edgerton, J. M. Liu, J. E. Shilling, D. O. Miller, W. Brune,

S. Schobesberger, E. L. D'Ambro and J. A. Thornton, Highly functionalized organic nitrates in the southeast United States: contribution to secondary organic aerosol and reactive nitrogen budgets, *Proc. Natl. Acad. Sci. U. S. A.*, 2016, **113**, 1516–1521.

102 J. M. O'Brien, P. B. Shepson, K. Muthuramu, C. Hao, H. Niki, D. R. Hastie, R. Taylor and P. B. Roussel, Measurements of alkyl and multifunctional organic nitrates at a rural site in Ontario, *J. Geophys. Res.: Atmos.*, 1995, **100**, 22795–22804.

103 J. M. O'Brien, P. B. Shepson, Q. Wu, T. Biesenthal, J. W. Bottenheim, H. A. Wiebe, K. G. Anlauf and P. Brickell, Production and distribution of organic nitrates, and their relationship to carbonyl compounds in an urban environment, *Atmos. Environ.*, 1997, **31**, 2059–2069.

104 C. Zuth, A. L. Vogel, S. Okenfeld, R. Huesmann and T. Hoffmann, Ultra-high-resolution mass spectrometry in real-time: atmospheric pressure chemical ionization orbitrap mass spectrometry (ApCI-Orbitrap-MS) of atmospheric organic aerosol, *Anal. Chem.*, 2018, **90**, 8816–8823.

105 A. E. Perring, S. E. Pusede and R. C. Cohen, An observational perspective on the atmospheric impacts of alkyl and multifunctional nitrates on ozone and secondary organic aerosol, *Chem. Rev.*, 2013, **113**, 5848–5870.

106 G. Socrates, *Infrared and Raman Characteristic Group Frequencies*, John Wiley & Sons, New York, 2001.

107 Q. Zhang, D. R. Worsnop, M. R. Canagaratna and J. L. Jimenez, Hydrocarbon-like and oxygenated organic aerosols in Pittsburgh: insights into sources and processes of organic aerosols, *Atmos. Chem. Phys.*, 2005, **5**, 3289–3311.

108 X. Zhang, R. C. Mcvay, D. D. Huang, N. F. Dalleska, B. Aumont, R. C. Flagan and J. H. Seinfeld, Formation and evolution of molecular products in alpha-pinene secondary organic aerosol, *Proc. Natl. Acad. Sci. U. S. A.*, 2015, **112**, 14168–14173.

109 R. Winterhalter, R. Van Dingenen, B. R. Larsen, N. R. Jensen and J. Hjorth, LC-MS analysis of aerosol particles from the oxidation of α-pinene by ozone and OH-radicals, *Atmos. Chem. Phys. Discuss.*, 2003, **2003**, 1–39.

110 B. Witkowski and T. Gierczak, Early stage composition of SOA produced by α-pinene/ozone reaction: α-acyloxyhydroperoxy aldehydes and acidic dimers, *Atmos. Environ.*, 2014, **95**, 59–70.

111 K. Kristensen, T. Cui, H. Zhang, A. Gold, M. Glasius and J. D. Surratt, Dimers in α-pinene secondary organic aerosol: effect of hydroxyl radical, ozone, relative humidity and aerosol acidity, *Atmos. Chem. Phys.*, 2014, **14**, 4201–4218.

112 K. Kristensen, Å. K. Watne, J. Hammes, A. Lutz, T. Petäjä, M. Hallquist, M. Bilde and M. Glasius, High-molecular weight dimer esters are major products in aerosols from α-pinene ozonolysis and the boreal forest, *Environ. Sci. Technol. Lett.*, 2016, **3**, 280–285.

113 K. S. Docherty, W. Wu, Y. B. Lim and P. J. Ziemann, Contributions of organic peroxides to secondary aerosol formed from reactions of monoterpenes with O_3, *Environ. Sci. Technol.*, 2005, **39**, 4049–4059.

114 H. Cavdar and N. Saracoglu, Synthesis of new β-hydroxy nitrate esters as potential glycomimetics or vasodilators, *Eur. J. Org. Chem.*, 2008, **2008**, 4615–4621.

115 B. Holger, S. Friedrich and S. Wolfram, Thermal decomposition of 2-ethylhexyl nitrate (2-EHN), *Int. J. Chem. Kinet.*, 2002, **34**, 34–38.

116 D. A. Day, P. J. Wooldridge, M. B. Dillon, J. A. Thornton and R. C. Cohen, A thermal dissociation laser-induced fluorescence instrument for *in situ* detection of NO_2, peroxy nitrates, alkyl nitrates, and HNO_3, *J. Geophys. Res.: Atmos.*, 2002, **107**, DOI: 10.1029/2001jd000779.

117 A. Zelenyuk, J. Yang, C. Song, R. A. Zaveri and D. Imre, A new real-time method for determining particles' sphericity and density: application to secondary organic aerosol formed by ozonolysis of α-pinene, *Environ. Sci. Technol.*, 2008, **42**, 8033–8038.

118 M. J. Ezell, S. N. Johnson, Y. Yu, V. Perraud, E. A. Bruns, M. L. Alexander, A. Zelenyuk, D. Dabdub and B. J. Finlayson-Pitts, A new aerosol flow system for photochemical and thermal studies of tropospheric aerosols, *Aerosol Sci. Technol.*, 2010, **44**, 329–338.

119 J. F. Pankow and W. E. Asher, SIMPOL.1: a simple group contribution method for predicting vapor pressures and enthalpies of vaporization of multifunctional organic compounds, *Atmos. Chem. Phys.*, 2008, **8**, 2773–2796.

120 B. Moller, J. Rarey and D. Ramjugernath, Estimation of the vapour pressure of non-electrolyte organic compounds *via* group contributions and group interactions, *J. Mol. Liq.*, 2008, **143**, 52–63.

121 Y. Nannoolal, J. Rarey, D. Ramjugernath and W. Cordes, Estimation of pure component properties: Part 1. Estimation of the normal boiling point of non-electrolyte organic compounds *via* group contributions and group interactions, *Fluid Phase Equilib.*, 2004, **226**, 45–63.

122 N. M. Donahue, W. Chuang, S. A. Epstein, J. H. Kroll, D. R. Worsnop, A. L. Robinson, P. J. Adams and S. N. Pandis, Why do organic aerosols exist? Understanding aerosol lifetimes using the two-dimensional volatility basis set, *Environ. Chem.*, 2013, **10**, 151–157.

123 A. D. Becke, A new mixing of Hartree–Fock and local density-functional theories, *J. Chem. Phys.*, 1993, **98**, 1372–1377.

124 J. P. Perdew, K. Burke and Y. Wang, Generalized gradient approximation for the exchange–correlation hole of a many-electron system, *Phys. Rev. B: Condens. Matter Mater. Phys.*, 1996, **54**, 16533.

125 T. H. Dunning Jr, Gaussian basis sets for use in correlated molecular calculations. I. The atoms boron through neon and hydrogen, *J. Chem. Phys.*, 1989, **90**, 1007–1023.

126 J. S.-Y. Yu, *α-Pinene organic nitrate synthesis, formation, and simulation*, Thesis Manuscript, 2010.

127 A. L. Lockwood, P. B. Shepson, M. N. Fiddler and M. Alaghmand, Isoprene nitrates: preparation, separation, identification, yields, and atmospheric chemistry, *Atmos. Chem. Phys.*, 2010, **10**, 6169–6178.

128 Y. Shao, Z. Gan, E. Epifanovsky, A. T. B. Gilbert, M. Wormit, J. Kussmann, A. W. Lange, A. Behn, J. Deng, X. Feng, D. Ghosh, M. Goldey, P. R. Horn, L. D. Jacobson, I. Kaliman, R. Z. Khaliullin, T. Kuś, A. Landau, J. Liu, E. I. Proynov, Y. M. Rhee, R. M. Richard, M. A. Rohrdanz, R. P. Steele, E. J. Sundstrom, H. L. Woodcock, P. M. Zimmerman, D. Zuev, B. Albrecht, E. Alguire, B. Austin, G. J. O. Beran, Y. A. Bernard, E. Berquist, K. Brandhorst, K. B. Bravaya, S. T. Brown, D. Casanova, C.-M. Chang, Y. Chen, S. H. Chien, K. D. Closser, D. L. Crittenden, M. Diedenhofen, R. A. DiStasio, H. Do, A. D. Dutoi, R. G. Edgar, S. Fatehi, L. Fusti-Molnar, A. Ghysels, A. Golubeva-Zadorozhnaya, J. Gomes, M. W. D. Hanson-Heine, P. H. P. Harbach, A. W. Hauser, E. G. Hohenstein, Z. C. Holden, T.-C. Jagau, H. Ji, B. Kaduk, K. Khistyaev, J. Kim, J. Kim, R. A. King, P. Klunzinger, D. Kosenkov, T. Kowalczyk, C. M. Krauter, K. U. Lao, A. D. Laurent, K. V. Lawler, S. V. Levchenko, C. Y. Lin, F. Liu, E. Livshits, R. C. Lochan, A. Luenser, P. Manohar, S. F. Manzer, S.-P. Mao, N. Mardirossian, A. V. Marenich, S. A. Maurer, N. J. Mayhall, E. Neuscamman, C. M. Oana, R. Olivares-Amaya, D. P. O'Neill, J. A. Parkhill, T. M. Perrine, R. Peverati, A. Prociuk, D. R. Rehn, E. Rosta, N. J. Russ, S. M. Sharada, S. Sharma, D. W. Small, A. Sodt, T. Stein, D. Stück, Y.-C. Su, A. J. W. Thom, T. Tsuchimochi, V. Vanovschi, L. Vogt, O. Vydrov, T. Wang, M. A. Watson, J. Wenzel, A. White, C. F. Williams, J. Yang, S. Yeganeh, S. R. Yost, Z.-Q. You, I. Y. Zhang, X. Zhang, Y. Zhao, B. R. Brooks, G. K. L. Chan, D. M. Chipman, C. J. Cramer, W. A. Goddard, M. S. Gordon, W. J. Hehre, A. Klamt, H. F. Schaefer, M. W. Schmidt, C. D. Sherrill, D. G. Truhlar, A. Warshel, X. Xu, A. Aspuru-Guzik, R. Baer, A. T. Bell, N. A. Besley, J.-D. Chai, A. Dreuw, B. D. Dunietz, T. R. Furlani, S. R. Gwaltney, C.-P. Hsu, Y. Jung, J. Kong, D. S. Lambrecht, W. Liang, C. Ochsenfeld, V. A. Rassolov, L. V. Slipchenko, J. E. Subotnik, T. Van Voorhis, J. M. Herbert, A. I. Krylov, P. M. W. Gill and M. Head-Gordon, Advances in molecular quantum chemistry contained in the Q-Chem 4 program package, *Mol. Phys.*, 2015, **113**, 184–215.

129 L. Martínez, R. Andrade, E. G. Birgin and J. M. Martínez, PACKMOL: A package for building initial configurations for molecular dynamics simulations, *J. Comput. Chem.*, 2009, **30**, 2157–2164.

130 M. J. Frisch, G. W. Trucks, H. B. Schlegel, G. E. Scuseria, M. A. Robb, J. R. Cheeseman, G. Scalmani, V. Barone, G. A. Petersson, H. Nakatsuji, X. Li, M. Caricato, A. Marenich, J. Bloino, B. G. Janesko, R. Gomperts, B. Mennucci, H. P. Hratchian, J. V. Ortiz, A. F. Izmaylov, J. L. Sonnenberg, D. Williams-Young, F. Ding, F. Lipparini, F. Egidi, J. Goings, B. Peng, A. Petrone, T. Henderson, D. Ranasinghe, V. G. Zakrzewski, J. Gao, N. Rega, G. Zheng, W. Liang, M. Hada, M. Ehara, K. Toyota, R. Fukuda, J. Hasegawa, M. Ishida, T. Nakajima, Y. Honda, O. Kitao, H. Nakai, T. Vreven, K. Throssell, J. A. Montgomery Jr, J. E. Peralta, F. Ogliaro, M. Bearpark, J. J. Heyd, E. Brothers, K. N. Kudin, V. N. Staroverov, T. Keith, R. Kobayashi, J. Normand, K. Raghavachari, A. Rendell, J. C. Burant, S. S. Iyengar, J. Tomasi, M. Cossi, J. M. Millam, M. Klene, C. Adamo, R. Cammi, J. W. Ochterski, R. L. Martin, K. Morokuma, O. Farkas, J. B. Foresman and D. J. Fox, *Gaussian 09, Revision A.02*, 2009.

131 F. B. van Duijneveldt, J. G. C. M. van Duijneveldt-van de Rijdt and J. H. van Lenthe, State of the art in counterpoise theory, *Chem. Rev.*, 1994, **94**, 1873–1885.

132 A. D. Becke, Density-functional thermochemistry. III. The role of exact exchange, *J. Chem. Phys.*, 1993, **98**, 5648–5652.

133 P. Stephens, F. Devlin, C. Chabalowski and M. J. Frisch, *Ab initio* calculation of vibrational absorption and circular dichroism spectra using density functional force fields, *J. Phys. Chem.*, 1994, **98**, 11623–11627.

134 R. Ditchfield, W. J. Hehre and J. A. Pople, Self-consistent molecular-orbital methods. IX. An extended gaussian-type basis for molecular-orbital studies of organic molecules, *J. Chem. Phys.*, 1971, **54**, 724–728.

135 S. Grimme, J. Antony, S. Ehrlich and H. Krieg, A consistent and accurate *ab initio* parametrization of density functional dispersion correction (DFT-D) for the 94 elements H-Pu, *J. Chem. Phys.*, 2010, **132**, 154104.

136 M. Shiraiwa, C. Pfrang, T. Koop and U. Pöschl, Kinetic multi-layer model of gas–particle interactions in aerosols and clouds (KM-GAP): linking condensation, evaporation and chemical reactions of organics, oxidants and water, *Atmos. Chem. Phys.*, 2012, **12**, 2777–2794.

137 J. Israelachvili, *Intermolecular & Surface Forces*, Academic Press, 2nd edn, 1991.

138 D. J. Donaldson, B. T. Mmereki, S. R. Chaudhuri, S. Handley and M. Oh, Uptake and reaction of atmospheric organic vapours on organic films, *Faraday Discuss.*, 2005, **130**, 227–239.

139 P. A. Vanderhoff, H. W. Thompson and R. A. Lalancette, Structure of (±)-*cis*-pinonic acid, *Acta Crystallogr., Sect. C: Cryst. Struct. Commun.*, 1986, **42**, 1766–1769.

140 K. Treves, L. Shragina and Y. Rudich, Measurement of octanol–air partition coefficients using solid-phase microextraction (SPME)—application to hydroxy alkyl nitrates, *Atmos. Environ.*, 2001, **35**, 5843–5854.

141 C. M. Boyd, T. Nah, L. Xu, T. Berkemeier and N. L. Ng, Secondary organic aerosol (SOA) from nitrate radical oxidation of monoterpenes: effects of temperature, dilution, and humidity on aerosol formation, mixing, and evaporation, *Environ. Sci. Technol.*, 2017, **51**, 7831–7841.

142 C. Pfrang, M. Shiraiwa and U. Pöschl, Chemical ageing and transformation of diffusivity in semi-solid multi-component organic aerosol particles, *Atmos. Chem. Phys.*, 2011, **11**, 7343–7354.

